3.15 Fundamentals of High-Pressure Homogenization of Foods

Juan C Osorio-Arias[a,b], Oscar Vega-Castro[a], and Sergio I Martínez-Monteagudo[c], [a] BIOALI Research Group, Food Department, Faculty of Pharmaceutical and Food Sciences, University of Antioquia, Medellin, Colombia; [b] Aoxlab Research Group, AOXLAB S.A.S, Development and Innovation Department, Medellin, Colombia; and [c] Dairy and Food Science Department, South Dakota State University, Brookings, SD, United States

3.15.1 Introduction

The homogenization of foods involves the dispersion of the structural elements (particles, molecules, globules, droplets, aggregates, granules, etc.) within a surrounding continuous material. Such dispersion of the individual elements is achieved by forcing a pumpable food to flow through a minute orifice, where the kinetic energy of the fluid is dissipated into energy absorbed, redistributed, and lost in the form of heat. The fluid experiences significant mechanical effects (shear, turbulence, and cavitation) that results in the dispersion of the individual structural elements.

Throughout the years, the homogenization of foods has evolved from a manufacturing step carried out in dairy plants to an established and essential unit operation, adopted in many fields. As a unit operation, homogenization performs multiple functions such as reduction of particle size, dissolution, mixing, dispersion, encapsulation, emulsification, and structuring. Currently, there are two major categories of homogenization technologies, commonly referred to as standard homogenization and high-pressure homogenization (HPH), with operating pressure levels up to 50 MPa and 300 MPa, respectively.

Over the past few years, research on the use of HPH has resulted in significant advancement in different aspects of the technology including, inactivation of enzymes, pasteurization, sterilization, extraction, cell disruption, stabilization of bioactive compounds,

micro-encapsulation, and others. The applications of high-pressure homogenization have led to a huge growth in the number of publications in peer-reviewed journals and conference proceedings. This chapter aims at providing a succinct overview of the historical progress of the technology, a review on the physics behind homogenization, an overview of the fundamentals of operating principles and configurations of different valves, and a summary of recent advances.

3.15.2 Historical Overview of Homogenization

Table 1 presents selected technological milestones of homogenization. More than 100 years ago, 1899–1904, Auguste Gaulin invented an apparatus for thoroughly mixing of milk (Gaulin, 1904). Gaulin's invention consisted of passing the milk through a series of capillary tubes by the action of a three-piston pressure pump. At the outlet of the capillary tubes, the milk collides with a concave valve controlled by a spring press. Soon after, the capillary tubes were replaced with a single small tube that created a gap, where the milk is forced to pass through. The gap concept had been the essential feature of homogenization over the years, and changes in the geometry of the gap have opened the door for new applications of homogenization. Gaulin's device was an improved version of early attempts on emulsification by forcing a liquid mixture through a tiny hole (Trout, 1950). Interestingly, the term intimacy mixing referred to the breakdown of fat globules, which results in a continuous and homogenous view under the microscope. Such observation brought up a new verb, homogenization, unknown up to that time. Gaulin's process was also known as fixation or fixed milk because the process yielded a fixed emulsion within a liquid.

In 1909, the first homogenizer was launched commercially by Manton-Gaulin Manufacturing Company in Boston, MA. Years later, the improvements in the homogenizer were focused on the transmission power and overall sanitation of the new equipment. Among the relevant innovations of homogenization was the introduction of the principle of opposite-current (1914), where the stream of milk was deflected by a sharp angle and reverted to pass the incoming milk, creating a shearing force (Trout, 1950). Another remarkable milestone during the development of homogenization was about 1910–1910 when the manufacture of evaporated milk incorporated the homogenization step (Hunziker, 1935). The homogenization of evaporated milk was added before canning to break up the fat globules and prevent them from rising to the top of the canned milk. Soon after, the superior quality of ice-cream manufactured with homogenization was discovered. Ice-cream formulation greatly benefited from the mixing and dispersing ability of the homogenization. Other advantages were also noticed, including more uniform and smoother texture, improved whipping ability, and a shorter aging period. By 1915–20, the ice-cream industry widely employed homogenization during the manufacture of ice-cream (Fisk, 1924). In subsequent years (1920–40), the adaptation of homogenization continued to expand leading to the introduction of homogenized milk in Canada (Trout, 1963). In subsequent years, homogenization became an essential step during the manufacture of evaporated and sweetened condensed milk, which prevented the separation of fat upon storage. Indeed, a common practice to prevent fat separation was to pass the concentrated milk through the homogenizer twice. By 1925, Gaulin's company introduced the two-stage homogenizer, a homogenization device with two valves in series (Innings, 2015). The significance of the two-stage homogenizer was the distinction between auxiliary parts and the homogenizing valve. This design

Table 1 Selected technological milestones in the development of homogenization

Year	*Milestones*	*References*
1892	Invention of emulsification process for artificial butter	Trout (1950)
1899–1904	Invention of an apparatus for stabilizing emulsions	Gaulin (1904)
1903	The concept of homogenization was introduced	Trout (1950)
1909	Manufacture of the first commercial homogenizer	Innings (2015)
1912	Invention of the opposite-current valve	Trout (1950)
1910–4	The manufacture of evaporated milk included homogenization	Hunziker (1935)
1915–20	Ice-cream manufacture incorporated the homogenization step	Fisk (1924)
1925	Invention of the two-stage homogenizer	Innings (2015)
1927	Homogenized milk was introduced in Canada	Trout (1963)
1930	Adjustable homogenizing valve	McClatchie (1930)
1934	Experiments on the effect of homogenization on curd tension	Theophilus et al. (1934)
1940	Studies on homogenization and lyposis of milk	Gould (1941)
1945	Manufacture of homogenizers for 4000 L h^{-1}	
1950	Studies on the cavitation during homogenization	Loo et al. (1950)
1961	Introduction of the aseptic homogenizer	Innings (2015)
1969	Invention of a process of the manufacture of peanut butter	Dzurik et al. (1969)
1982	Invention of the micro-gap valve	Pandolfe (1982)
1993	Invention of high-pressure homogenization pasteurization of juices	Clack et al. (1993)

led to a better understanding of the physics behind homogenization. In 1930, the invention of an adjustable valve for homogenizing devices (McClatchie, 1930), along with the two-stage homogenizer marked a significant milestone that allows accommodating large volumes by adjustable valves without the need of multiple passes.

The effects of homogenization on flavor, oxidation, sedimentation, curd tension, nutritive value, and physical properties were documented through the middle part the 20th century (1930–60). By 1934, it was demonstrated that the application of homogenization significantly reduced the curd tension of milk (Theophilus et al., 1934). The softness of the curds was attributable to the increase in the number of globules serving as points of weakness in the coagulum and to a lesser extent, to the casein adsorption on the increased fat surface area. In addition to the softness of the curds, their size was also reduced which increased the total surface area. Such observations led to the belief that the process made the milk more suitable for infant feeding, a claim not supported by scientific evidence in the 1930s (Trout, 1950). Early observations on homogenized milk for infant feeding were unsatisfactory. Years later, Doan (1938) questioned the experimental evidence on the curd tension value of milk as a satisfactory index of digestibility. In subsequent years (1935–40), the pressure levels required for reducing the curd tension were determined. Homogenized milk at 13 MPa reduced the curd tension, and beyond that pressure there was marginal reduction (Trout, 1950). Soon after, it was shown that the homogenization of raw milk rapidly and significantly increased the lipolysis of milk fat (Gould, 1941). Such increment on the free fatty acids was due to lipolytic action.

In the 1940s, the homogenizers transitioned from a proof-of-concept carried in few places to an established unit operation adopted in multiple plants. By 1945, the homogenizers were designed to handle streams of up to 4000 L h^{-1} at pressure levels of up to 30 MPa. The presence of cavities in homogenization was first reported by Loo et al. (1950), who pointed out a hissing noise occurring during the regular operation of the homogenizer. Such a hissing noise was further related to the cavitation phenomenon in a flow. When the product reaches the vena contracta at the valve clearance, cavities are formed in regions of high velocity and low pressure. During 1960's, the use of homogenizers spread beyond the dairy industry, finding applications in lubricants, textiles, biotechnology, and pharmaceutical industries. In 1961, the manufacture of long shelf-life milk brought the development of aseptic homogenizer to ensure that fat droplets were small to minimize the Brownian motion. Another remarkable milestone for homogenization was the invention of a process for the production of peanut paste containing particles of a maximum size of 80 μm (Dzurik et al., 1969). Over the years, the homogenization valve was under constant changes in terms of geometry and design. The valve designs included single service valves, tapered valves, grooved (stepped) valves, grooved valves, highly chamfered, or knife-edge valves. Such changes and modifications were oriented toward producing smaller particles with less energy. In 1982, the invention of the Gaulin Micro-Gap valve proved to be 30% more efficient than the conventional valves. The efficiency of the Micro-Gap valve lies in three crucial considerations of the design: (i) short travel distance, (ii) small gap, and (iii) optimum backpressure. More importantly, these considerations were the foundations for a new generation of homogenization valves, where the liquid is forced to pass through a small geometry creating pressure levels in the range of hundred MPa. In the early 1990s, the effects of homogenization pressure at levels of 100–250 MPa were investigated on inactivation of enzymes and microorganisms, mixing, emulsification, and particle size reduction. By 1993, an invention for the pasteurization of orange juice employed pressure levels of 100 MPa using an APV Gaulin homogenizer (Clack et al., 1993). In subsequent years, the homogenization valves for high-pressure become a reality with the introduction of a new generation of valves from different manufacturers. Examples of such valves are counter-jet microchannel, radial-diffuser, and axial-flow through orifice valves (Martinez-Monteagudo et al., 2017). Nowadays, high-pressure homogenization has found applications beyond dairy manufacturing including, enzyme and microbial inactivation of juices and beverages, cell disruption for biotechnology purpose, mixing and dispersion of pumpable liquids, emulsification and encapsulation, and protein modification.

3.15.3 Physics of Fluid Food Homogenization

Homogenization is the physical process of subdividing large particles into a large number of smaller particles having a small size (Walstra, 1993). **Fig. 1** illustrates the homogenization process, where the subdivision involves the disruption of the large particles and the dispersion of the newly created particles. The entire process occurs within the homogenization valve, and the overall efficiency depends on the specific design of the valve and flow conditions. Despite a large number of available valves, the homogenization is generally described by the combined effect of main factors:

(i) Shearing effects.
(ii) Hydrodynamic cavitation.
(iii) Turbulence.

3.15.3.1 Shearing Effects

Inside the homogenization valve, the liquid is forced to flow through a minute gap that disrupts the normal motion of the fluid, creating shearing actions. The created shear actions occur within the fluid itself and between the fluid and valve seat. Velocities of up to 200–300 m s^{-1} are typically achieved through a 100 μm gap. The shear action within the fluid is planar stress, in one direction, while the shear between the large particles and the surface of the valve is characterized by extensional flow stress. Both shearing actions play critical roles during the disruption of particles under a laminar flow regime, according to a dimensionless number

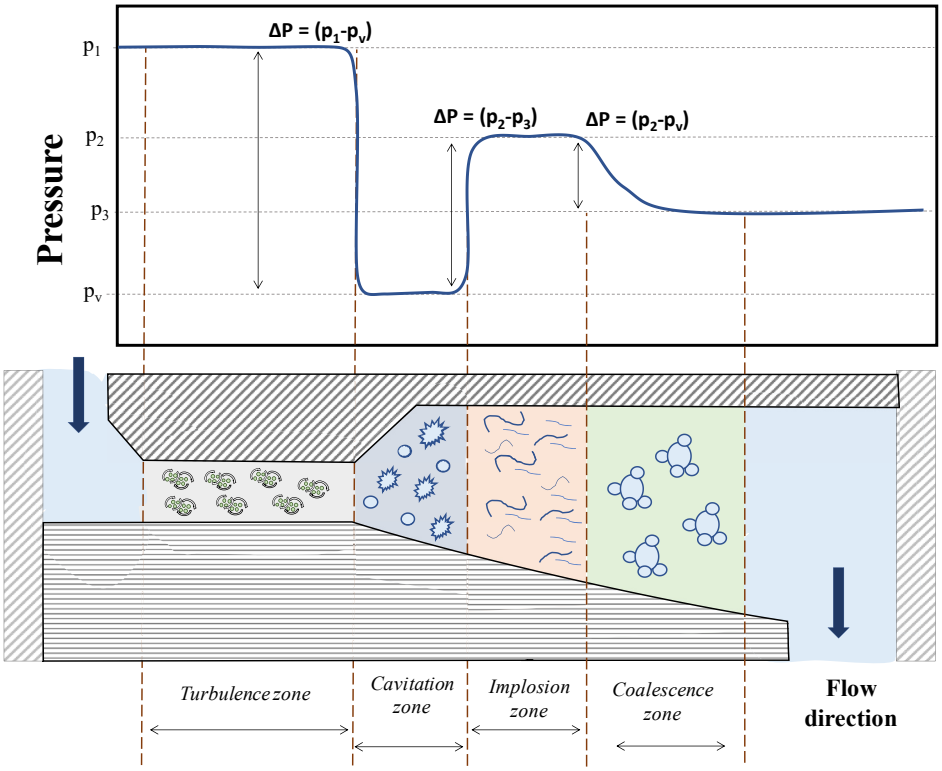

Figure 1 Illustration of the homogenization mechanism of a hypothetical homogenization valve. The corresponding time scale of the different zones is for illustration purpose.

known as Weber number (*We*, **Eq. 1**). Walstra (1993) characterized the stress exerted on a drop of oil-in-water emulsion in laminar flow using the *We* as it relates inertial and surface forces.

$$We = \frac{\rho \cdot v^2 \cdot l}{\gamma} \tag{1}$$

Where ρ is the density of the fluid (kg m^{-3}); v is the velocity (m s^{-1}); l is a characteristic length (m); and γ is the surface tension (N m^{-1}). During homogenization, the *We* have been used to establish a critical value, We_{cr}, for disruption of droplets in laminar flow. As the pressure increases, the value of We_{cr} must be considered cautiously because the surface tension is strongly affected by pressure and temperature, according to the thermodynamic relation (**Eq. 2**):

$$\left(\frac{\partial \gamma}{\partial p}\right)_{T,\ A,} = \left(\frac{\partial V}{\partial A}\right)_{p,T} \tag{2}$$

Where γ – surface tension; p – pressure; V – total volume of the system; A – total surface area. The right side of **Eq. (2)** represents the change in volume per unit area of the interface. **Eq. (2)** is derived from the fundamental equations of thermodynamics for free energy and free enthalpy (Eggers, 2012). A closer inspection of **Eq. (2)** reveals that pressure will reduce the surface tension when molecular concentration occurs as a result of the applied pressure. On the other hand, an increase in surface tension will occur when the volume contraction of the continuous phase overcomes the attractive forces in the interfacial volume. The effect of pressure on surface tension has been demonstrated by Michaels and Hauser (1951), who measured the interfacial tension of hydrocarbons and water under pressure and found that cyclic molecules were positively adsorbed within the interfacial layer while branch molecules were negatively adsorbed. Studies on the effect of high-pressure on the surface tension of immiscible liquids for food applications have not been reported.

3.15.3.2 Hydrodynamic Cavitation

The term cavitation refers to the process of formation of cavities within the liquid, their growth, and subsequent collapse when the pressure of the liquid is suddenly reduced below its vapor pressure (Carlton, 2012). Cavitation is responsible for issues such as erosion, noise, and vibration, which lead to malfunction of many machineries and pumps. The collapse of vapor bubbles on the metal surface is known to cause localized stresses of high amplitude wearing the surfaces of the homogenizer gap (Innings et al., 2011).

The underlying physics of cavitation is based on the pressure-volume relationship of the van der Waals equation, and the theory of probability of fluctuation (Endo, 1994). During the transition from liquid to vapor, there is an interphase where both phases coexist, which corresponds to the length of the spinodal line of stability of the liquid. The probability of fluctuation theory predicts that the frequency of cavitation is proportional to the pressure fluctuation within the liquid. Overall, two kinds of cavitation are thought to occur when a fluid experience cavitation, acoustic and hydrodynamic (Ferrari, 2017). Hydrodynamic cavitation is the second type of cavitation, and it is the main effect in nozzles and discharge orifices. The formation of cavities during homogenization of milk was earlier reported by Loo et al. (1950), who suggested that cavities were formed in regions of high velocity and low pressure. The formation of vapor bubbles and their subsequent collapse can cause shattering effects (Håkansson et al., 2010). Shirgaonkar et al. (1998) suggested that cavitation generates shock waves causing cell disruption, and the magnitude of the disruption was related to the homogenization pressure. The violent collapse of the cavities can also generate free radicals (Gogate et al., 2001), accelerating reactions such as ionization of potassium iodide (Naidu et al., 1994), hydrolysis of fatty acids and oxidation (Gogate et al., 2001; Suslick et al., 1997) (**Table 1**).

The dynamics of the cavitation depends on the flow conditions, fluid properties, surrounding pressure, and the geometry of the valve. Over the last decade, significant progress has been made in the fundamental understanding of hydrodynamic cavitation. Experiments concerning hydrodynamic cavitation have led to identifying critical parameters, including pressure coefficient (C_p), minimum pressure coefficient (C_{pmin}), cavitation appearance (C_{app}), cavitation number (C_v), cavitation inception (C_{in}), and Thoma number (T_h). **Table 2** shows some parameters used for the characterization of hydrodynamic cavitation. The pressure coefficient (C_p) relates the ratio of pressure forces to inertial forces, and it is only a function of the geometry of the valve for a given fluid. This is an important parameter for designing homogenization valves and discharge orifices. In the absence of cavitation, the fluid velocities and the pressure coefficient are independent of the magnitude of pressure. Thus, an increase in the inlet pressure will result in an equal change in all other forces, and consequently the C_p is unaffected. For a given liquid flowing through a homogenization valve, there will be a particular location at which the pressure is the minimum ($p_{min} \approx p_v$). Such relation is known as minimum pressure coefficient (C_{pmin}), and it is expressed by **Eq. (4)** (**Table 2**). C_{pmin} varies only with the geometry of the valve for a given liquid. The value of C_{pmin} helps to establish the minimum pressure needed at which the cavitation would first appear. **Eq. (4)** can be mathematically manipulated to yield another relevant parameter, cavitation appearance (C_{app}). Accordingly, C_{app}, the appearance of the cavitation is only a function of the velocity of the fluid for a given valve, fluid, and temperature.

The appearance of cavitation has been mostly quantified and predicted using two dimensionless numbers, cavitation number (C_v) and cavitation inception (C_{in}) (**Eqs. 5 and 6**, respectively **Table 2**). C_v and C_{in} characterize how close the pressure in the liquid is to the vapor pressure, and therefore the potential for cavitation. As the value of C_v decreases, cavitation will first appear at some particular value of C_v known as the incipient cavitation number. The C_v at which cavitation begins is called the critical cavitation number. Above this value, cavitation does not occur, and below the critical number, cavitation occurs, and further reduction of the C_v results in an increase in the number and size of the vapor cavities. In a multicomponent flow, the cavity pressure is the sum of the partial pressure of the vapor of the liquid and of any gases that may have been introduced into the cavity. C_{in} has been used to predict cavitation onset in homogenizers (Kumar and Pandit, 1999). In contrast, C_v is not normally used in homogenizers; instead the Thoma number (T_h, **Eq. 8**, **Table 2**) is used for the analysis of cavitation (Innings et al., 2011), which is defined as the relation of outlet and inlet pressure. Commercial homogenizers usually operate within a T_h number of 0.1 to 0.3. Ideally, T_h and C_{in} can be used to improve the design of homogenization valve by locating the cavitation as a function of operating conditions. However, experimental evidence showed that the onset of cavitation was not clearly identified in standard homogenizers (Shirgaonkar et al., 1998). Shirgaonkar et al. (1998) suggested that C_v and C_{in} cannot be correlated with certainty because the intensity of cavitation depends on the geometry of the valve and the homogenization pressure. This has been shown by Floury et al. (2004), who simulated the cavitation number, C_v, during high-pressure homogenization and found that C_v decreased with homogenization pressure with an estimated value of 0.005 for a pressure of 340 MPa. The C_v obtained by Floury et al. (2004) is smaller compared to that typically reported in homogenization processes (pressure levels up to 30 MPa) where cavitation is expected to occur when the C_v is near to 1.0. Håkansson et al. (2010) located the region of cavitation as a function of operating conditions by measuring the light scattered from cavitation bubbles. These authors found that cavitation bubbles grow

Table 2 Key parameters for the characterization of hydrodynamic cavitation

Parameter	*Symbol*	*Equation*	*Equation number*
Pressure coefficient	C_p	$C_p = \frac{p_1 - p_2}{1/2 \cdot \rho \cdot v_i^2}$	(3)
Minimum pressure coefficient	C_{pmin}	$C_{pmin} = \frac{p_{min} - p_2}{1/2 \cdot \rho \cdot v_i^2}$	(4)
Cavitation appearance	p_{app}	$p_{app} = p_v + 1/2 \cdot \rho \cdot v_i^2$	(5)
Cavitation number	C_v	$C_v = \frac{p_2 - p_1}{1/2 \cdot \rho \cdot v_i^2}$	(6)
Cavitation inception	C_{in}	$C_{in} = \frac{p_{app} - p_v}{1/2 \cdot \rho \cdot v_i^2}$	(7)
Thoma number	T_h	$T_h = \frac{p_1 - p_v}{p_2 - p_1}$	(8)

p_2 is the downstream pressure; p_1 is the upstream pressure, p_v is the vapor pressure of the liquid; v_{max} is the maximum velocity.

and collapse in the valve gap, and their intensity increased with the homogenization pressure and decreased when a second homogenization stage or backpressure was used.

The C_v is derived from a dimensional analysis of a flow around an obstacle, where the pressure at any point (p_M) can be written as a function of the incidence angle of the flow relative to the obstacle (α), pressure (P_∞) and velocity (V_∞) of the flowing liquid, density (ρ) and viscosity (μ), according to **Eq. (9)**:

$$P_M = f(P_\infty,\ \alpha,\ \rho,\ \mu,\ V_\infty) = \frac{P_\infty - p_v}{1/2\,\rho V_\infty^2} \tag{9}$$

Such a definition of cavitation suggests that any pressure in the liquid is essential only in terms of the pressure difference (Chahine, 1997). The inception of cavitation in a liquid at pressures near the vapor pressure requires the presence of nuclei, which contain minute amounts of vapor. The understanding and predictability of bubble nucleation is an active area of research (Carlton, 2012).

Cavitation will occur only when enough nuclei become unstable and grow when subjected to a pressure reduction. The growth conditions have been mathematically derived from the analysis of the static equilibrium conditions for a spherical nucleus (**Fig. 2**A). The internal forces, produced by the partial pressures of the gas and vapor within the nucleus, must be balanced by the ambient pressure and the surface-tension pressure at the nucleus-liquid interface. The static equilibrium condition occurs when the ambient pressure plus the surface-tension pressure equal the vapor pressure plus the gas pressure, **Eq. (10)**:

$$P_A + \frac{2\gamma}{R_o} = p_v + \frac{constant}{R^3} \tag{10}$$

where P_A is the ambient pressure, γ is the surface tension, R_o is the initial radio of the nuclei, p_v is the vapor pressure of the liquid, and R is the radio of the unstable nuclei. A graphical illustration of **Eq. (10)** is given in **Fig. 2**B, where the pressure adjacent to the bubble has reached a minimum value, below the vapor pressure of the liquid. A stable nucleus is obtained (indicated in the left-hand portion of the curve) when the ambient pressure is above the minimum value, and the initial bubble radius is smaller than a critical value. On the contrary, the bubble becomes unstable and grows without bound when the ambient pressure drops below the critical value. The extent of the transition between stable and unstable nuclei depends on the purity of the liquid. For instance, the presence of dissolved air forms cavities at pressure levels higher than the vapor pressure itself. Unstable nuclei produce bubbles of microscopic size and subsequently collapse due to the return of high pressure in their vicinity. Collapsing mechanisms of cavitation bubbles have been reviewed elsewhere (van Wijngaarden, 2016). In general, the collapse of the cavitation bubbles occurs within a very short timespan (milli- or micro-seconds), resulting in shockwaves that raise the liquid temperature. The numerical value of the temperature rise is of technological interest, and it depends on the pressure differential and viscosity of the liquid. The most common method for describing the collapse of bubbles is the Rayleigh model, where the bubble is defined using a spherical coordinate system whose origin is at the center of the bubble. The Rayleigh model for bubble collapse has led to a series of interesting results, including the existence of infinite velocities and pressures at the point of collapse. However, such interpretations must be taken cautiously due to the number of assumptions used for the Rayleigh model.

3.15.3.3 Turbulence

In a typical high-pressure homogenization, the fluid passage is abruptly reduced up to 100–1000-fold. Such reduction generates velocity gradients of large magnitude alongside with irregular motions within the fluid in time and space, which are characteristics

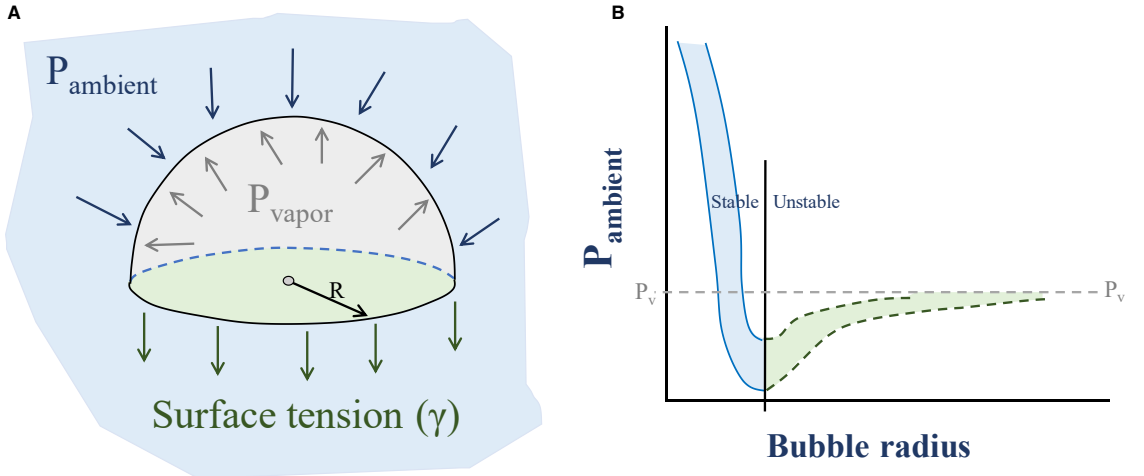

Figure 2 Schematic illustration of the forces acting on a cavitation bubble nucleus (A), and conditions for static equilibrium of cavitation nuclei (B).

of turbulent flow (Tennekes and Lumley, 1972). At the discharge point within the homogenization valve, the resulting flow has been characterized as a turbulent flow, where it displays unpredictable random patterns in which the fluid particles undergo complicated paths, causing different mixing zones within the fluid. Such mixing zones enhance diffusivity and, therefore, increase the rates of momentum, heat and mass transfer (Rosa, 2006). Thus, the existence of turbulence in homogenization enhanced mixing, dispersion, and emulsification (Martinez-Monteagudo et al., 2017).

Turbulent flows are dissipative, meaning that their kinetic energy is dissipated in the form of eddies and heat. Mechanistically, viscous shear stresses increase the internal energy of the fluid at the expense of kinetic energy of turbulence. Turbulence is a continuous phenomenon that cannot maintain itself unless a constant source of energy is supplied (Tennekes and Lumley, 1972). These characteristics of turbulent flows provide the required energy for particle break-up and redistribution as well as temperature increase. During homogenization, the energy provided to the system is dissipated in a spectrum of eddies or vortices of different intensities and length scales in energy cascade process. In a cascade process, the inertial term is responsible for the transfer of energy to smaller and even smaller scales until it reaches a small enough scale, where the viscosity becomes predominant. At the smallest scale, the kinetic energy is dissipated into heat. The sequence of the cascade process has been described by Kolmogorov's theory, which assumes that only liquid droplets larger than the smallest dissipating-eddies will break-up. Kolmogorov's theory has been described by Hinze (1955), who developed the theory of maximum size ($d_{\max}$) that a drop can withstand in turbulent flow. Mathematically this can be expressed as follows:

$$d_{max} \approx \varepsilon^{-0.4} \gamma^{0.6} \rho^{-0.2} \tag{11}$$

Where ε is the average amount of energy dissipated per time. The maximum size of a particle and energy has been studied during the emulsification of milk and other food products (Walstra, 1993). An investigation on the emulsification of paraffin oil showed that the rate of energy dissipation correlated with the maximum diameter of droplets that resist break-up (Davies, 1985). Such a relationship assumed that velocity fluctuations due to turbulence are the same in all directions and can be characterized by the Kolmogorov theory. Davies' relationship is only valid within the pressure range of 3–14 MPa and high Reynolds numbers (R_e), ~30,000. Mohr (1987) studied the emulsification of oil-in-water dispersions using different homogenization valves, including flat, diffuser, edge-type, and nozzle valves. The dispersion of droplets within the turbulent flow occurred as primary and secondary dispersion. The primary dispersion is controlled by eddies of high energy content, which is influenced by the geometry of the homogenization valve. The secondary dispersion occurred when the particles are larger than the smallest energy-dissipating eddies. Floury et al. (2004) simulated the velocity profiles for water within a high-pressure homogenization valve operated at constant flow rate of 10 L h^{-1} and a maximum pressure of 350 MPa. The turbulence intensity, a measure of the turbulence strength, increased with the homogenization pressure from ~10% to ~34% at 26 and 340 MPa, respectively, and the maximum turbulence intensity was found at the exit of the valve gap. The location of the maximum turbulence intensity is of great interest in the performance of the homogenization valve. It should be highlighted that the turbulence intensity reported by Floury et al. (2004) occurred within the laminar regime in the upstream, gap, and downstream parts of the valve. Most of the HPH units commercially available are laboratory-scale handling flow rates of less than 10 L h^{-1} under laminar regime. Parameters such as turbulence intensity and length scale are useful for equipment sizing and rating during the scale-up of HPH units where turbulence regime is desired.

3.15.4 Mechanisms of Homogenization

The exact mechanism of the break-up of particles is somewhat disputed with shear actions, implosion of cavitation bubbles, and interactions with turbulent eddies (Håkansson et al., 2009). The extent to which each of these factors contributes to the homogenization process depends on the valve geometry and design, equipment size, temperature, pressure, and fluid viscosity. Nevertheless, the effects of turbulent interactions have consensually regarded as the main source for particle break-up and further dispersion. The influence of the different actions is schematically illustrated in **Fig. 1**. On entering the gap (p_1), the flow is accelerated to such an extent that the pressure is reduced to p_v over a very short distance. The pressure drop results in the development of a cavitation zone. The single-phase liquid flow in the turbulent zone is then converted into a two-phase vapor-liquid flow in the cavitation zone. Velocities of above 100 m s^{-1} are developed in the two-phase liquid; a supersonic flow. In radial diffuser valves, a pressure build-up occurs by the reduction in the flow rate that leads to the implosion of the cavitation bubbles and, thus, to a sudden transition from supersonic to subsonic flow. In the zone of implosion, energy is generated which is responsible for dispersion. The exact position of the active region has been an area of debate. Detailed studies showed no fragmentation in the gap instead droplets are elongated until reaching a position outside of the gap, where the particles break-up by turbulent inertial force.

3.15.5 Homogenizers

Fundamentally, a high-pressure homogenizer is a hydraulic pump equipped with a discharge port and a homogenization valve. In a way, high-pressure homogenizers are power-generating devices designed to convert mechanical kinetic energy into hydraulic potential energy. The hydraulic pump system within the homogenizer intakes the fluid at atmospheric pressure to fill a predetermined volume of space inside the homogenizer through an inlet port and subsequently discharges pressurized fluid by reducing

the volume of space at an output chamber. The hydraulic pump produces only the flow, while the operating pressure is determined solely by the reduction of volume space at the discharge point. The hydraulic system consists of a high-pressure pump connected to a smooth rod, which is driven by a powerful electric motor. For large homogenizers, the high-pressure pump normally consists of three to five pistons providing a constant flow of pressure fluid (Innings, 2015). **Fig. 3** illustrates a three-piston homogenizer. The fluid to be homogenized enters from the homogenizer (number (1) in **Fig. 3**) due to the action of the piston pump. Then, the flow passes a set of check valves and continuous to the first homogenization valve, and subsequently into the second homogenization stage. A homogenizer operated with a piston pump generates a pulsating flow that can accelerate and decelerate the liquid, creating pulsation within the upstream and downstream pipes of the homogenizer (Innings, 2015). A pulsating flow is a result of pressure variations that in extreme cases results in breakage of the pipes. Another consequence of the pulsation is the distortion of the control system of the homogenizer. **Fig. 3** illustrates a typical large-scale homogenizer (2000–3000 L h^{-1} at pressure levels of up to 50 MPa. High-pressure homogenizers operate under the same principle. Currently, some manufacturers such as APV (Crawley, UK, www.spxflow.com), Avestin (Ottawa, Canada, www.avestin.com), Bee International (Easton, MA, USA, www.beei.com), Gea Niro Soavi (Parma, Italy, www.gea.com), Stansted Fluid Power Ltd (Harlow, UK, www.stanstedfluidpower.com), and Ypsicon (Barcelona, Spain, www.ypsicon.com) have industrial-, pilot-, or lab-scale devices able to exert homogenizing pressures between 100–400 MPa with a flow range between 100–1500 L h^{-1}.

3.15.6 Valve Design

The design of the homogenization valves broadly consists of flowing a liquid through a narrow gap between a valve rod and a seat, which accelerates fluid velocity. The flow travels a predetermined distance before it impacts on valve walls or impact rings, where it is deflected by a certain angle; generating intense energy changes. The efficiency and functionality of the valves depend on their design and geometry (Martinez-Monteagudo et al., 2017). Homogenization valves can be found in a number of types and configurations, depending on the final application. The existing literature reveals hundreds of patents granted for homogenization valves (Pandolfe, 1982). Schultz, Wagner, Urban, and Ulrich (2004) provided a detailed description of the most common types of homogenization valves. High-pressure valves made of ceramic seats and needles capable of withstanding pressure levels from 100 to 400 MPa are classified into counter-jet, radial diffusers, and axial flow valves. **Table 3** summarizes the characteristics of the most common high-pressure valves in terms of their design, operating pressure, and flow rate.

3.15.6.1 Counter-Jet Valve

Fig. 4 illustrates a counter-jet valve used in high-pressure homogenizers. This type of valve is based upon the impingement of two turbulent flows. The flow stream is divided into two microchannels, where the fluid velocity is accelerated around 10-fold. Then, the two streams are forced under pressure to frontally impinge (Cook and Lagase, 1985). The impingement takes place within a small space known as the interaction chamber. The pressure is discharged by directing the fluid to an outlet of around 9-fold bigger than the diameter of the microchannels. The original design of the valve was invented in 1985, and since then, there have been some modifications in its design in order to increase the volume stream. **Fig. 4**B–E illustrates the currently available counter-jet valves.

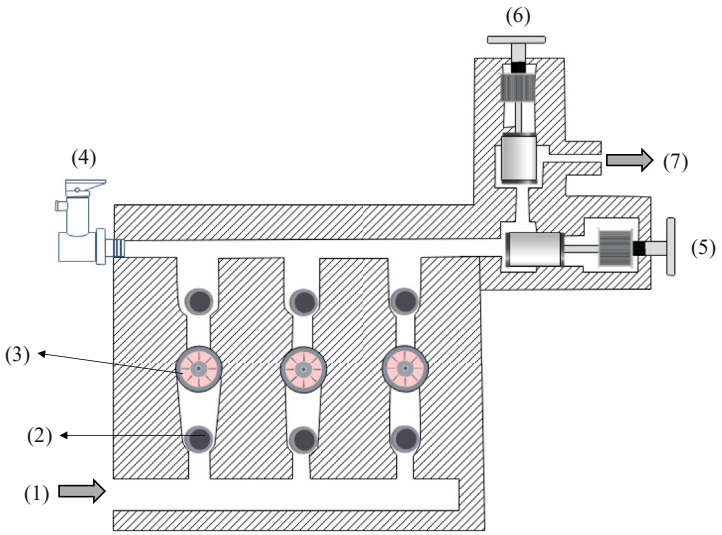

Figure 3 Schematic illustration of a three-piston pump with two homogenization valves. (1) product inlet; (2) ball valve; (3) piston; (4) safety valve; (5) first homogenization stage; (6) second homogenization stage; (7) product outlet.

Table 3 Characteristics of selected high-pressure homogenization valves

Type of valve	*Manufacturer*	*Pressure range*	*Volume streams*	*Characteristics*
Counter-jet microchannel	Microfluidizer® Processors	Up to 150 MPa	- Lab scale ($<$10 L h^{-1})	- No movable parts - Flow rate controls the operating pressure
Counter-jet microchannel	AVESTIN, Inc.	Up to 200 MPa	- Lab scale ($<$20 L h^{-1}) - Pilot scale (50–160 L h^{-1}) - Industrial scale (1000 L h^{-1})	- No movable parts - Flow rate controls the operating pressure
Radial-diffuser annular valve	GEA Niro Soavi	12–150 MPa	- Lab scale ($<$10 L h^{-1}) - Industrial scale (5000 L h^{-1})	- Flow rate depends on the operating pressure - Temperature rise 17 °C per 100 MPa for water
Radial-diffuser annular valve	APV (Now SPX Flow Technology)	Up to 150 MPa	- Lab scale ($<$10 L h^{-1}) - Pilot scale (90 L h^{-1}) - Industrial scale (800 L h^{-1})	- Flow rate depends on the operating pressure - Pressure is controlled by adjusting the gap size (75–15 μm)
Axial-flow through orifice valve	Stansted Fluid Power Ltd	Up to 400 MPa	- Lab scale ($<$10 L h^{-1}) - Pilot scale (90 L h^{-1})	- Constant flow rate - Pressure is controlled by adjusting the gap size ($<$10 μm) - Temperature rise 20 °C per 100 MPa for water

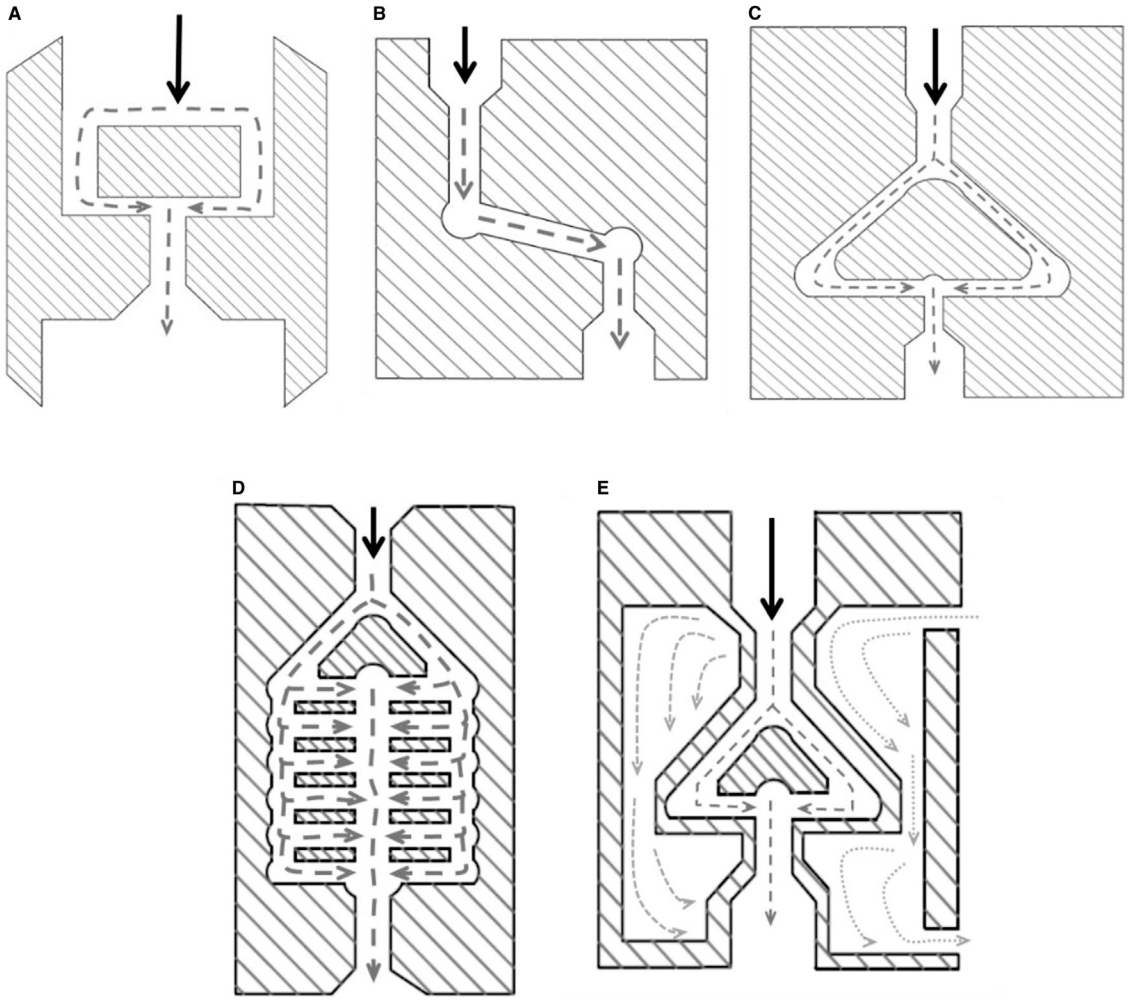

Figure 4 Schematic representation of a high-pressure counter-jet valve: (A) Microchannel valve; (B) Jet to wall or Z-chamber type valve; (C) Jet to jet or Y-chamber type valve; (D) Multi-slotted Y-chamber; (E) microchannel valve with cooling system. Drawings do not represent real scale.

Jet to wall valve or Z-chamber (Fig. 4B) was designed to minimize wall shearing and reducing the rise in temperature while effectively producing micro-emulsion (Panagiotou and Fisher, 2012). The jet to jet valve or Y-chamber (Fig. 4C and D) was developed to increase the volume stream since multiple channels can be incorporated, resulting in a multi-slotted Y-chamber. Y-chamber valves yield a more uniform droplet size distribution than Z-chamber valves (Panagiotou and Fisher, 2012). Fig. 4E shows a design for a Y-chamber valve in which cooling of the liquid is performed inside the chamber. Counter-jet valves offer the advantage of not having movable parts, which simplifies the operation. For scaling up, multiple channels can be incorporated to increase throughput. Industrial-scale units capable of handling volume streams up to 1000 L h^{-1} at 200 MPa are commercially available. However, industrial volume streams at pressure levels higher than 200 MPa would require high flow rates and, therefore a great amount of energy input through the pumping system. This is the principal disadvantage of counter-jet valves since they are designed to control the homogenization pressure only using the flow rate.

3.15.6.2 Radial Diffuser Valve

In general, radial diffuser valves consist of an axial valve face and a mobile valve seat, where the homogenization pressure is controlled by adjusting the slit width and the upstream flow rate (Schultz et al., 2004). Fig. 5A illustrates a high-pressure radial diffuser valve where the upstream flow first passes through a nozzle with the radial profile before entering the impact chamber, which consists of two consecutive coaxial annular chambers (Grandi and Gandini, 2006). Such design allows pressure levels of up to 150 MPa by only increasing the flow rate - even at industrial scale. Grandi and Gandini (2006) reported that increasing the size and the number of homogenization valves failed to achieve satisfactory results in terms of homogenizer performance and emulsion quality. Radial diffuser valves are available for lab- and industrial-scale within the pressure range of 0.1 to 150 MPa.

Fig. 5B illustrates a high-pressure radial diffuser valve formed by stacking disk-shaped valve members. The upstream flow enters the valve through holes located at the bottom of each stacked member. The pressurized fluid travels through annular grooves formed between the surfaces of each valve member, and it is forced out through a narrow gap formed at the end of the annular

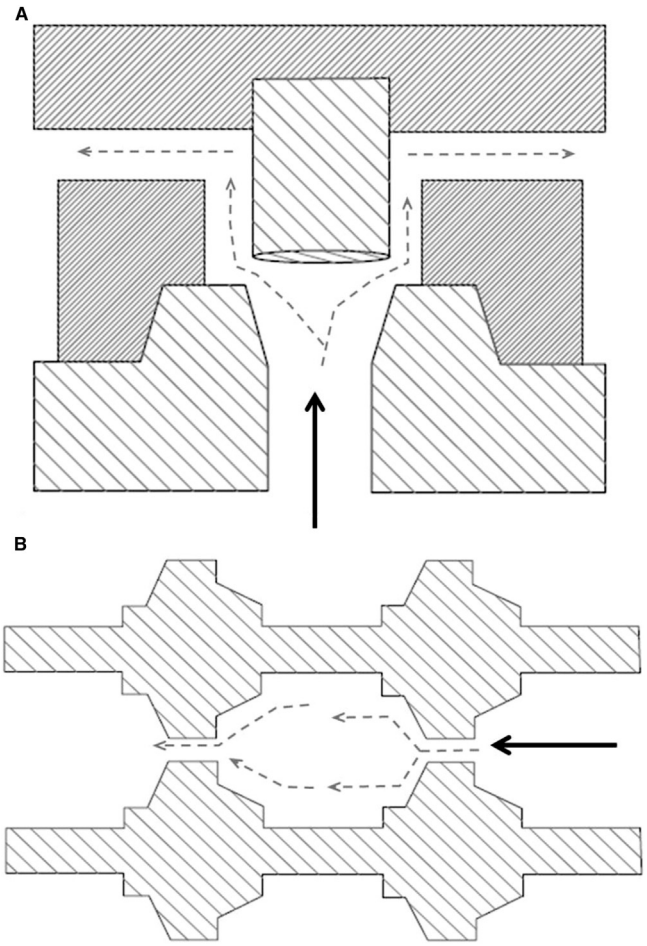

Figure 5 Schematic diagram of (A) a high-pressure radial diffuser valve (B) stacking of high-pressure radial diffuser valve. Drawings do not represent real scale.

groove (Kinney et al., 1999). The distance between the inlet hole and the gap is chamfered providing knife edges, and it connects to a high-pressure chamber. The gap connects axially with an outlet; a pipe of larger diameter. This design has the advantage of accommodating industrial volume streams by adding more valve members to the stack. The gap size can be pneumatically adjusted by moving a top plug piston, which compresses the stack members (Kinney et al., 1999).

3.15.6.3 Axial-Flow Through Orifice Valve

Fig. 6 shows a schematic diagram of an axial-flow through orifice valve. The pressurized fluid enters the homogenization valve axially, where the diameter of the inlet pipe is reduced 3-fold. Such reduction increases fluid velocity that travels a distance of <2 mm until it collides with a needle and valve seat. A tiny gap with a slit width of <10 μm and length of <2.5 mm is formed between the needle and the annular valve seat. When the fluid reaches the low-pressure region outlet pipe, it is considered downstream. The pressure is only controlled by the gap slit, and it can be manipulated by moving the needle closer to the valve seat which narrows the gap slit. A pneumatic actuator is used to move forward or retract the needle. This valve offers the advantage of operating at various pressures with a constant flow rate. The flow rate is dictated by the intensifier capacity. This type of valve is currently available for lab- and pilot-scale volume streams.

3.15.7 Engineering Considerations

3.15.7.1 Gap Size

The size of the homogenization gap is of great relevance for the performance of the homogenizer. Fundamentally, the fluid should travel the shortest distance within the smallest possible volume. Such an idea involves physical constraints where the geometry of the valve is the main factor affecting the pressure drop. Table 4 summarizes the approaches used to mathematically represent the pressure drop across the homogenization valve. Equations shown in Table 4 are simplified expressions aimed at calculating pressure gradients in a homogenization valve. Analysis of laminar flow between parallel disks has been examined by Nakayama (1964), who developed an empirical equation for predicting pressure loss across nozzles considering friction loss and discharge velocity losses. Similarly, Kawaguchi (1971) developed an empirical equation that predicts pressure loss in radial turbulent flow between parallel discs. These two equations were developed for nozzles using dimensionless numbers in which the pressure loss due to friction depends on the valve design (knife-type, sharp-edge, chamfered, etc.). Phipps (1975) challenged the applicability of such equations and found that such theoretical expressions for energy losses are not entirely applicable to homogenization valves. Phipps (1975) substituted some empirical relationships to yield an equation, which has been used to predict pressure drop in homogenizers. Kleinig and Middelberg (1997) developed an equation based on the hypothesis that the maximum pressure gradient occurs at the entrance of the valve gap where pressure is quickly converted to kinetic energy. Pressure drop takes place over a small region corresponding to the turbulence length scale, which itself depends on the valve geometry. Kleinig and Middelberg (1997) validated their results with CFD simulations, and their equation has been used to relate pressure drop with the degree of disrupted cells. Rovinsky (1994) calculated pressure drops in a radial diffuser valve using the Borda equation for sudden expansion of a flow. However, the total pressure drop at high-pressure levels cannot be accurately calculated because significant recirculation develops

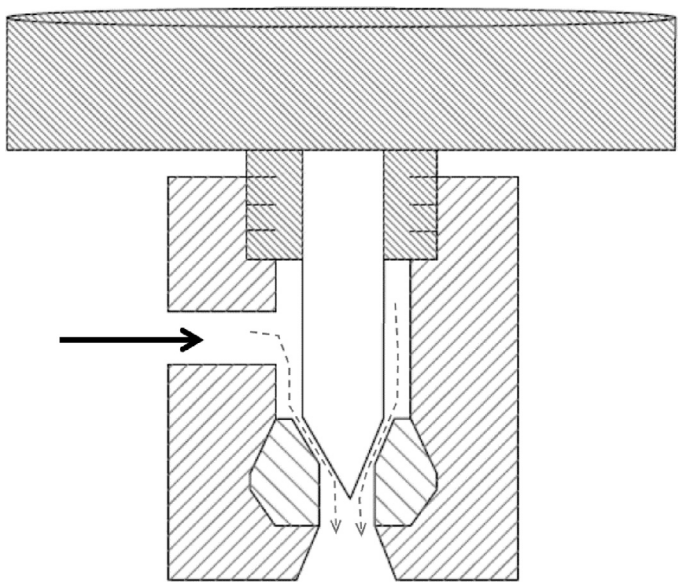

Figure 6 Schematic diagram of an axial-flow through orifice valve. Drawings do not represent real scale.

Table 4 Mathematical models describing pressure drop across selected homogenization valves

Valve type	*Equation*	*References*
Nozzle parallel discs	*Laminar regime* $\Delta p_L = f_L \cdot \frac{\rho}{2} \cdot \left[\frac{Q}{2 \cdot \pi \cdot r_i \cdot h}\right]^2 + \frac{6 \cdot \mu \cdot Q}{\pi \cdot h^3} \cdot ln\left(\frac{r_e}{r_i}\right) + \frac{54 \cdot \rho}{70} \cdot \left[\frac{Q}{2 \cdot \pi \cdot r_e \cdot h}\right]^2$	Nakayama (1964)
Nozzle parallel discs	*Turbulent regime* $\Delta p_T = f_T \cdot \frac{\rho}{2} \cdot \left[\frac{Q}{2 \cdot \pi \cdot r_i \cdot h}\right]^2 + \frac{0.00336 \cdot \rho \cdot v^{\frac{1}{4}}}{h^3} \cdot \left[\frac{Q}{\pi}\right]^{7/8} \cdot \left[\frac{1}{r_i^{\frac{3}{4}}} - \frac{1}{r_e^{\frac{3}{4}}}\right] + \frac{64 \cdot \rho}{126} \cdot \left[\frac{Q}{2 \cdot \pi \cdot r_e \cdot h}\right]^2$	Kawaguchi (1971)
Radial-diffuser annular valve	*Turbulent regime* $\Delta p = \frac{8}{4} \cdot \left[\frac{Q}{2 \cdot \pi \cdot r_i \cdot h}\right]^2 + \frac{5 \cdot \rho \cdot v^{\frac{3}{5}}}{h^3} \cdot \left[\frac{Q}{2 \cdot \pi}\right]^{7/5} \cdot \left[\frac{1}{r_i^{\frac{2}{5}}} - \frac{1}{r_e^{\frac{2}{5}}}\right] + \frac{\rho}{2} \cdot \left[\frac{Q}{2 \cdot \pi \cdot r_e \cdot h}\right]^2$	Phipps (1975)
Radial-diffuser annular valve	*Turbulent regime* $\frac{\Delta p}{L} = \frac{\rho \cdot Q^2}{8 \cdot \beta \cdot \pi^2 \cdot r_i^2 \cdot h^5}$	Kleinig and Middelberg (1997)
Radial-diffuser annular valve	$\Delta p = \frac{v^2}{2} \cdot \left(\frac{A_2}{A_1} - 1\right)^2$	Rovinsky (1994)
Radial-diffuser annular valve	$\frac{2 \cdot \Delta p}{\rho \cdot \bar{u}^2} = k_i + k_f + k_e$	Stevenson and Chen (1997)
Radial-diffuser annular valve	$\Delta p = 6.67\ x\ 10^6 \cdot p \cdot \mu^2 - 9.0\ x\ 10^7 \cdot p \cdot \mu + 3.83\ x\ 10^8 \cdot p - 1.73\ x10^2 \cdot \mu^2 + 1.94x\ 10^{11} \cdot \mu - 5.77\ x\ 10^{11}$	Kelly and Muske (2004)

when flow experiences a sudden change in area, making it difficult to calculate this loss from a volume analysis. Stevenson and Chen (1997) calculated the pressure drop in a radial diffuser. They considered the total pressure drop as the sum of the entrance, exit, and frictional loss, which were based on empirical relationships, and the applicability of such an equation was validated with CFD simulation. Kelly and Muske (2004) derived an empirical equation from CFD simulation. Kelly and Muske's equation is expressed as a function of fluid viscosity and homogenization pressure, and it has shown good agreement with the degree of cell breakage. The applicability of Phipps's equation was tested by Floury et al. (2004), who expressed the pressure drop as a function of the valve slit in a lab-scale HPH (axial-flow through orifice valve). Floury et al. (2004) measured the thickness of water-suspended wax grits after homogenization (10 MPa) to estimate the distance between the valve and the valve seat. Interestingly, the distance agreed with the estimated values from Phipps's equation. Donsì, Ferrari, Lenza, and Maresca (2009) compared the pressure drop in a lab-scale and pilot-scale HPH (axial-flow through orifice valve) using Phipps's equation. Significant differences were found during pressure drop with increasing flow rate. Casoli, Vacca, and Berta (2010) established a relation between flow rate and operating pressure in a homogenizer operated at industrial scale.

Overall, the homogenization valves are designed to accommodate relatively large volumes within a constrained space or geometry. Thus, the analysis of the gap size and its relation with pressure is an essential area of research. The majority of the high-pressure valves are somewhat radial, which makes it difficult to interpret the relationship between gap height and homogenization pressure. **Fig. 7** illustrates the area of the gap and homogenization pressure in an axial-flow through orifice valve. The solution is fed axially into the valve (flow upstream in **Fig. 7**A), where it is accelerated between the needle and the valve seat. The opening or gap between the needle and the valve seat is known as the gap space. Then, the solution emerges from the gap space, and it impacts the walls of the valve seat. The gap space is the only operating variable, and its shape resembles a flat cone (**Fig. 7**B). Decreasing the gap space increases the operating pressure and the mechanical forces associated with it.

3.15.7.2 Flow Patterns

The flow pattern in a homogenizer is made up of all averaged velocities occurring within the flow, possessing magnitude and direction. Such velocities include macroscopic characteristics (by passing, dead zones, recirculation, and plug flow) and fine-scale characteristics (turbulence) (Bałdyga and Pohorecki, 1995). Emulsification, mixing, and reduction of particle size occur in the homogenization valve under the influence of hydrodynamic forces, and analysis of the flow patterns within the homogenization valve has been a topic of engineering and scientific interest (Håkansson et al., 2012). Experimental methods for determining flow patterns during homogenization are somewhat challenging to implement due to the high velocities generated in a very short distance or gap length. Alternatively, computational fluid dynamics (CFD) has been used for the analysis of flow patterns during

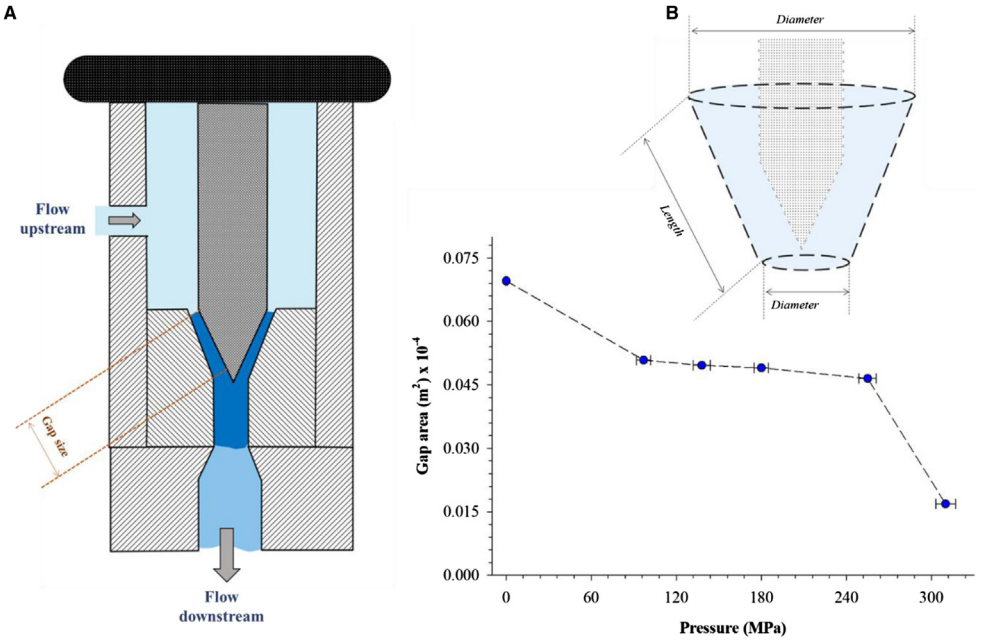

Figure 7 Illustration of the gap area and pressure relation in an axial-flow through orifice valve. (A) Schematic drawing of the valve, and (B) representation of the calculated area based on the geometry.

homogenization. The governing equations originate from classical mechanics and conservation laws, and they have been analyzed in great detail in classic textbooks (Tennekes and Lumley, 1972). Briefly, CFD models consist of solving the Reynolds-Averaged Navier-Stokes equations using turbulence models under the Boussinesq hypothesis. Such approach relies heavily on empirical assumptions, and validation with experimental data should be performed.

Table 5 summarizes studies aimed to characterize flow patterns during homogenization. Kleinig and Middelberg (1997) used a laminar and a turbulent CFD model to describe the velocity profile in a radial diffuser annular valve. These authors found a parabolic velocity profile for both regimes. Stevenson and Chen (1997) used computational fluid dynamics to construct velocity profiles in the valve gap. A rapid acceleration in the valve gap was followed by the quick development of velocity profiles. Large velocity

Table 5 Velocity profile and flow patterns in selected high pressure homogenization valves

Turbulence model	*Type of valve*	*Characteristic*	*References*
- Laminar - High *Re k-ε*	Radial diffuser annular valve	Parabolic velocity profile: - Laminar $v_{max} = \left[\frac{81}{3200}\cdot\frac{Q^4}{\mu\cdot h^2\cdot r_e^2\cdot\pi^4}\right]^{1/3}\cdot\left[r^3 - r_e^3 + \frac{3\cdot Q\cdot r_e\cdot h}{50\cdot\pi\cdot\mu}\right]^{-1/3}$ - Turbulent $v_{max} = \frac{Q}{2\cdot\pi\cdot r_e\cdot h}\cdot\left[\frac{1.32\cdot r_e\cdot h}{m\cdot r\cdot(r-r_e)}\right]^{1/2}$	Kleinig and Middelberg (1997)
- Standard k-ε	Radial diffuser annular valve	Large velocities gradients across the gap	Stevenson and Chen (1997)
- Standard k-ε - RNG k-ε - Realizable k-ε	Radial diffuser annular valve	Maximum velocity was influenced by the operating pressure and fluid viscosity	Miller et al. (2002)
- RNG k-ε	Axial-flow through orifice valve	Parabolic velocity profile $v = \frac{3\cdot Q}{4\cdot\pi\cdot y\cdot h}\cdot\left[1 - \left(\frac{2\cdot x}{h}\right)^2\right]$	Floury et al. (2004)
- Standard k-ε	Radial diffuser annular valve	Sudden acceleration in the gap and flow detachment at the outlet of the gap	Casoli et al. (2010)
- Standard k-ε	Microchannel	Location of cavitation: $\frac{p_v - p}{\rho} + \frac{p_{G0}}{\rho}\cdot\left(\frac{R_0}{R}\right)^3 = R\frac{d^2R}{dt^2} + \frac{3}{2}\left(\frac{dR}{dt}\right)^2 + \frac{4\mu}{R\rho}\frac{dR}{dt} + \frac{2\gamma}{\rho R}$	Håkansson et al. (2010)

gradients were also found across the valve, creating recirculation zones between the impact ring and the valve seat. The existence of a recirculation zone has been associated with agglomeration of particles. Another CFD model showed that the maximum channel velocity increases with pressure, and it was affected by the fluid viscosity (Miller et al., 2002). Floury et al. (2004) analyzed the flow patterns in an axial-flow through orifice valve of HPH. The velocity at the entrance of the gap increases rapidly with the operating pressure, reaching values of 100 m s^{-1} at 340 MPa. It was predicted that a high-velocity profile would develop afterward, with velocities up to 200 m s^{-1} at the highest operating pressure (340 MPa). A fully parabolic velocity profile was developed inside the valve gap. Large velocity gradients were generated near the walls of the gap. At the exit of the gap, the fluid velocity rapidly decreases over a short distance from 80 m s^{-1} to 0.6 m s^{-1}. This is an important difference between radial-diffuser and counter-jet valves. Similarly, a sudden acceleration in the gap entrance reaching velocities of 210 m s^{-1} was obtained from numerical simulation of an industrial-scale homogenizer (25 MPa and 18,000 L h^{-1}) (Casoli et al., 2010). These authors also reported flow detachment at the outlet of the gap, which was explained by the presence of cavitation. Innings and Trägårdh (2005) captured a series of pictures from the fluorescent light emitted from the sample. These authors observed drop formation, deformation, and break-up using a flat valve of a homogenizer (18 MPa). Emulsion drops were formed under a laminar regime with velocities of 1 m s^{-1}. Elongation of emulsion drops occurred at the entrance of the gap where velocities of 3 m s^{-1} were observed. Subsequent break-up took place at velocities of 8 m s^{-1} when the size of the emulsion drop reaches the smallest eddy. Similar observations were reported by Innings and Trägårdh (2007), who built a scale model homogenizer to measure velocity profiles and found a steady acceleration at the gap entrance. Their velocity measurements showed the maximum elongation rates occurred in the gap inlet. Håkansson et al. (2010) located the cavitation zone by building pressure and velocity profiles with CFD models and further validated their findings with acoustic measurements.

The applicability of CFD models heavily relies on empirical assumptions. Indeed, Håkansson et al. (2012) compared the literature for the analysis of fluid dynamics in homogenization valves in terms of turbulence models used and assumptions made in CFD models. These authors concluded that the flow patterns at the entrance of the gap can be accurately modeled regardless of the turbulence model. In the gap region, the use of more refined k-ε models is recommended. Interestingly, the models used for CFD were unable to describe the flow patterns of the turbulent region in the downstream of the valve gap.

3.15.7.3 Dissipation of Energy

During high-pressure homogenization, the temperature of the food material increases as a result of the heat of compression during isostatic pressure processing and temperature increase (turbulence and cavitation) in the fluid as it is being discharged through homogenization valve. Limited information is available on heat of homogenization and other physical and thermal properties (e.g., viscosity, thermal diffusivity, ionic strength, and others) of liquid foods during continuous flow HPH treatment.

Although the heat of compression and the heat generated during homogenization increase with the applied pressure, their governing principles are quite different. **Table 6** attempts to differentiate between the heat of compression and the heat generated during homogenization. The heat of compression is a result of decreasing the intermolecular distance between adjacent molecules during hydrostatic compression (Balasubramaniam et al., 2015), while the heat generated after the first homogenization stage is due to dissipation of kinetic energy as a result of thermo-mechanical discharge through homogenization valve. Another important difference is that the rise in temperature due to heat of compression is reversible upon decompression, while the rise in temperature due to the heat generated during homogenization is irreversible and is not maintained unless a continuous source of energy is supplied.

The increase in temperature during HPH is a critical parameter to consider during high-pressure homogenization. **Table 7** summarizes linear or polynomial based empirical models reported in the literature to estimate temperature increase during HPH. The models can be represented by **Eq. (12)**:

$$T_p = T_{in} + \alpha p + \beta p^2 \tag{12}$$

The constant term T_{in} represents the initial product temperature at which the authors conducted the experiments. Such empirical model parameters do not have any physical meaning and are valid only within experimental conditions (and geometry) employed

Table 6 Differences of temperature increase due to heat of compression during high pressure processing vs dissipation of kinetic energy during high-pressure homogenization

Parameters	*Heat of compression during high pressure process*	*Heat generated during high pressure homogenization*
Mode of pressure application	Hydrostatic pressure	Discharge through valve
Principle	Reduction of intermolecular distance (e.g. 15% reduction of water volume at 600 MPa)	Dissipation of kinetic energy
Temperature rise	- 3–8 °C/100 MPa - Reversible upon decompression	- 15–18 °C/100 MPa - Irreversible
Factors	- Composition - Pressure - Product initial temperature	- Pressure - Valve design

Table 7 Empirical models for predicting the temperature increase during high-pressure homogenization

Food matrix	*Type of valve*	*Equations*	*References*
Calf rennet solution	Radial-diffuser annular valve	$T = 0.18 * p + 23.55$ $23°C \leq T \leq 57°C$ 50 MPa $\leq p \leq$ 190 MPa	Leite Júnior et al. (2014)
Enzyme solution	Radial-diffuser annular valve	$T = 0.11 * p + 29.64$ $29°C \leq T \leq 54°C$ 50 MPa $\leq p \leq$ 200 MPa	Tribst and Cristianini (2012c)
Apple juice	Axial-flow through orifice valve	$T = -0.00018 * p^2 + 0.225 * p + 25.75$ $25°C \leq T \leq 88°C$ 50 MPa $\leq p \leq$ 350 MPa	Kumar et al. (2009)
Apple and carrot juice	Axial-flow through orifice valve	$T = -0.00018 * p^2 + 0.225 * p + 25$ $30°C \leq T \leq 84°C$ 50 MPa $\leq p \leq$ 350 MPa	Pathanibul et al. (2009)
Cell suspension	Axial-flow through orifice valve	$T = -0.0002 * p^2 + 0.2279 * p + 22.24$ $22°C \leq T \leq 75°C$ 50 MPa $\leq p \leq$ 350 MPa	Taylor et al. (2007)

T – temperature achieved during homogenization (°C); p – homogenization pressure (MPa).

in specific study. It is not clear whether heat loss during HPH is considered by authors when developing these models. Thiebaud, Dumay, Picart, Guiraud, and Cheftel (2003) observed that the inlet temperature in an axial-flow through orifice valve did not influence the rise in temperature due to the dissipation of kinetic energy. These authors found a ΔT ($T_p - T_{in}$) of ~ 15 °C per 100 MPa, regardless of the T_{in} (4, 14, or 24 °C). Similarly, Martinez-Monteagudo et al. (2017) demonstrated that the magnitude of the ΔT ($T_p - T_{com}$) was not affected by T_{in}, which was evaluated from 18 to 90 °C (**Fig. 8**). In the models reported in **Table 7**, the contribution of the heat of compression cannot be separated from the heat generated due to the dissipation of kinetic energy of a turbulent flow. Alternatively, a more generalized form of the equation (**Eq. 13**) can be used to estimate process temperature (T_p).

$$T_p = T_{in} + \delta * \Delta p + \xi * \Delta p - \sum heat\ loss \tag{13}$$

T_{in} corresponds to the inlet or preheating temperature, and it can be controlled with a heat exchanger. δ is the heat of compression of the fluid (Patazca et al., 2007) subjected to hydrostatic pressure (ΔP). The term ξ is the heat of homogenization that can be

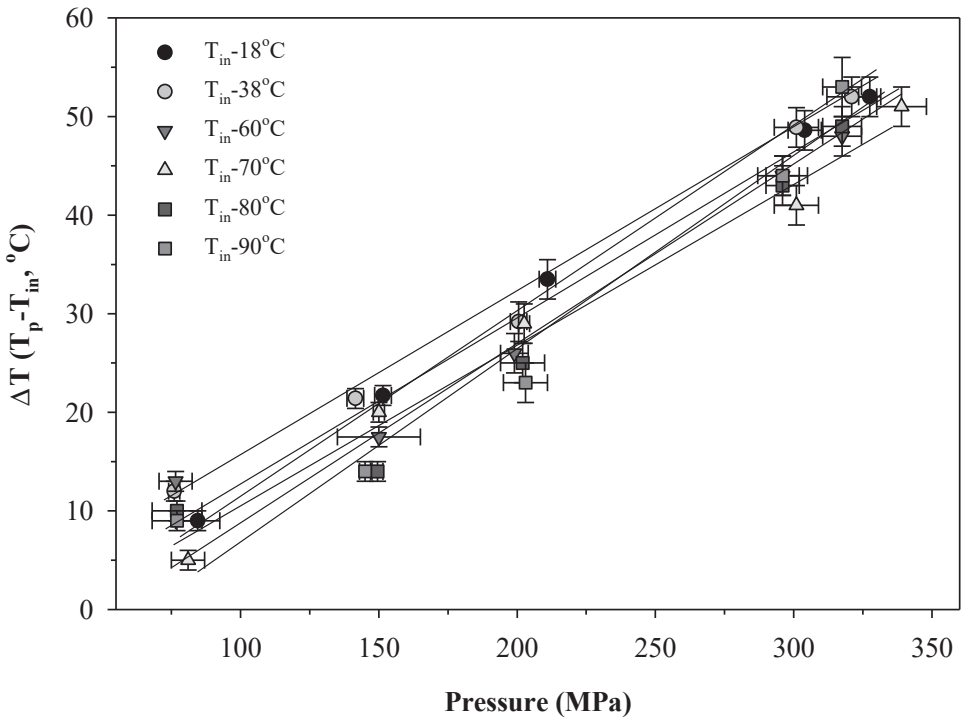

Figure 8 Effect of inlet temperature on the rise in temperature during high-pressure homogenization. T_{in} – inlet temperature; T_p – product temperature.

experimentally determined for specific valve geometry (Fig. 8). The heat losses are negligible when proper insulation is used. The dissipation of kinetic energy of turbulent flow can be divided into energy absorbed, redistributed and lost through heat. Interestingly, from the total turbulent kinetic energy only a small amount is lost through heat while the rest is absorbed and redistributed by the interaction of turbulence patterns of different scales.

3.15.8 Applications of High-Pressure Homogenization

Homogenization refers to the spatial redistribution of materials in order to achieve uniform macroscopic properties. Such redistribution may influence the properties of a given food product and the rate at which those changes proceed. This would be the case if the homogenization alters the molecular-scale of the reactants involved, which would modify their reactivity. During homogenization, the fluid experiences intense turbulence of different length scales; meso- and micro-scales. Turbulent micro-mixing theory deals with aspects of mixing which causes homogeneity on the molecular level (Bałdyga and Pohorecki, 1995). Micro-mixing is the last of the turbulent mixing stages consisting of viscous deformation of fluid elements, followed by molecular diffusion. The analysis of chemical reactions at the micro-mixing scale can be described from a Eulerian and turbulent framework. Unlike hydrostatic pressure where the effects of pressure on chemical reactions have been described by Le Chatelier's principle and transition state theory (Martinez-Monteagudo and Saldaña, 2014), the effects of dynamic pressure on chemical reactions are largely unknown. The following sections summarize the effects of high-pressure homogenization in ensuring microbial safety and quality of processed foods.

3.15.8.1 Microbial Inactivation

Microbiological inactivation during HPH treatment is influenced by a variety of factors including intensity of pressure, process temperature, residence time distribution or the number of passes (in the laboratory equipment), HPH valve design parameters as well as product characteristics (pH, composition, viscosity). Table 8 summarizes the studies conducted on HPH efficacy on various microorganisms. It is worth to note that modest HPH treatment (e.g., 200 MPa, $< 50\ ^{\circ}C$) is sufficient for inactivation of vegetative microorganisms. On the other hand, inactivation of bacterial spores requires intensive pressure-thermal treatment (e.g., 200 MPa and $> 100\ ^{\circ}C$). Many of these studies were conducted with laboratory HPH equipment provided by commercial vendors. Minimal efforts have been made to understand the influence of HPH equipment components (including HPH valve geometry and hold tube) in controlling microbiological efficacy of the treatment. Such information is needed for process scale-up and validation studies.

3.15.8.1.1 Fluid Viscosity

The effect of fluid viscosity on microbial inactivation has been studied by Diels et al. (2005a), who treated *E. coli* MG1655 suspensions of different viscosities. It was found that bacterial inactivation decreased with increasing the viscosity of the suspensions. At the valve gap, the fluid is subjected to non-isobaric (pressure drop) and non-isothermal (temperature rise due to dissipation of kinetic energy) conditions. Kelly and Muske (2004) empirically correlated the pressure drop at the exit of the valve gap as a function of fluid viscosity and homogenization pressure. Unfortunately, the thermal effect was not considered in Kelly and Muske's model. It is believed that non-isobaric and non-isothermal conditions strongly affect the viscosity of the fluid and, therefore the microbial inactivation. Thus, changes in product viscosity should be carefully considered when designing experiments for microbial inactivation.

3.15.8.1.2 Residence Time

Earlier researchers attempted to relate the HPH microbiological efficacy with the passage time of the fluid as it is discharged from the HPH valve. At the entrance of the valve gap, the velocity of the fluid is greatly accelerated, and the passage time through the valve is expected to be extremely short. Indeed, Walstra (1993) calculated passage time to be roughly $< 1\ \mu s$ for water flowing through a homogenizer (flat valve). Such extremely short passage times make it very difficult to evaluate the temperature-time combinations yielding desirable inactivation of microorganisms. Nevertheless, the exit of the homogenization valve, where the highest temperature is reached and the velocity of the fluid decreases, can be considered to be the beginning of the holding tube. Already, Amador Espejo et al. (2014) considered the holding section after the fluid passed through the homogenization valve and calculated a residence time of <0.5 s using the pipe diameter and flow rate. Amador Espejo et al. (2014) inactivated 6-log of *Bacillus* spores in milk held for <0.5 s at $140\ ^{\circ}C$ using a homogenization pressure of 300 MPa (Table 8). Similarly, Georget et al. (2014) calculated a residence time of 0.24 s after the homogenization valve during inactivation of *B. subtilis* PS832 (5-log). Likewise, Dong et al. (2015) inactivated 3-log of *B. amyloliquefaciens* in milk using an estimated residence time of 0.24 s. It seems reasonable to extend the distance between first and second homogenization stages in order to obtain residence times comparable to those employed in UHT (>4 s). In summary, HPH process time can be defined as the time at which the fluid food is held at the target temperature (in the hold tube section) during treatment.

3.15.8.1.3 Temperature

The fluid temperature within HPH systems is an important variable influencing microbiological inactivation efficiency. The temperature profile depends on the configuration of the HPH system. Taylor et al. (2007) attempted to separate the thermal contribution

Table 8 Summary of studies on the microbial efficacy of high-pressure homogenization

Strain	*Matrix*	*Reduction*	*Conditions*	*Type of valve*	*References*
Escherichia coli					
K-12	Apple juice and apple cider with chitosan	7-log	$T_{in} = 25$; $p = 250$; $T_p = 70$	Axial-flow through orifice valve	Kumar et al. (2009)
K-12	Saline solution	7-log	$T_{in} = 5$; $p = 300$; $T_p = 60$	Axial-flow through orifice valve	Taylor et al. (2007)
K-12	Apple and carrot juice	5-log	$T_{in} = 4$; $p = 250$; $T_p = 80$	Axial-flow through orifice valve	Pathanibul et al. (2009)
K-12 MG1655	PBS buffer (pH 7)	6-log	$T_{in} = 25$; $p = 250$–300; $T_p = 41$	Counter-jet	Diels et al. al. (2005a,b)
MG1655	Skim, soy and strawberry-raspberry milk	3.5-log/skim 3.0-log/soy 3.0-log/straw-rasp milk	$T_{in} = 25$; $p = 300$; $T_p = 41$	Counter-jet	Diels et al. (2005a,b)
MG1655 LMM1010	PBS buffer (pH 7)	5-log	$T_{in} = 25$; $p = 300$; $T_p = 42$	Counter-jet	Wuytack et al. (2002)
0157:H7 ATCC 35150	PBS buffer (pH 7)	8-log (after 3 passes)	$T_{in} = 25$; $p = 200$; FR = 1.5	Counter-jet	Vachon et al. (2002)
0157: H7 ATCC35150	PBS buffer (pH 7) Orange juice	6-log (after 6 passes)	$T_{iin} = 25$; $p = 200$	Counter-jet	Tahiri et al. (2006)
MG1655	PBS buffer (pH 7)	7-log	$T_{in} = 50$; $p = 250$; $T_p = >70$	Counter-jet	Diels et al. (2004)
058:H21 ATCC 10536 0157:H7 CCUG 44857	Orange juice	3.9-log (058:H21) 3.7-log (0157:H7)	$T_{in} = 20$; $p = 300$; FR = 18	Axial-flow through orifice valve	Briñez et al. (2006a)
Listeria innocua* and *Listeria monocytogenes					
ATCC 51742	Apple and carrot juice	5-log	$T_{in} = 4$; $p = 300$; $T_p = 80$	Axial-flow through orifice valve	Pathanibul et al. (2009)
ATCC 33090	Milk and orange juice	2.7-log	$T_{in} = 20$; $p = 300$; $FR = 18$	Axial-flow through orifice valve	Briñez et al. (2006b)
Not reported	PBS buffer (pH 7)	5-log	$T_{in} = 25$; $p = 300$; $T_p = 42$	Counter-jet	Wuytack et al. (2002)
LSD 105–1	PBS buffer (pH 7)	8-log (after 3 passes)	$T_{in} = 25$; $p = 200$; $FR = 1.5$	Counter-jet	Vachon et al. (2002)
Staphylococcus aureus* and *S. carnosus					
ATCC 13565	Milk and orange juice	Milk: 3.6-log Orange juice: 4.2-log	$T_{in} = 20$; $p = 300$; $FR = 18$	Axial-flow through orifice valve	Briñez et al. (2007)
CECT 976	Milk	7-log	$T_{in} = 20$; $p = 330$; $FR = 16$	Axial-flow through orifice valve	López-Pedemonte et al. (2006)
Not reported	PBS buffer (pH 7)	3-log	$T_{in} = 50$; $p = 300$;	Counter-jet	Diels et al. (2003)
Not reported	PBS buffer (pH 7)	6-log	$T_{in} = 25$; $p = 300$; $T_p = 42$	Counter-jet	Wuytack et al. (2002)
CECT 4491	Orange juice	4.8-log	$T_{in} = 20$; $p = 300$; $FR = 18$	Axial-flow through orifice valve	Briñez et al. (2007)
Salmonella					
Typhimurium	PBS buffer (pH 7)	3-log	$T_{in} = 25$; $p = 250$	Counter-jet	Wuytack et al. (2002)
serotype enteritidis ATCC 13047	PBS buffer (pH 7)	8-log (after 5 passes)	$T_{in} = 25$; $p = 200$; flow = 1.5 L h^{-1}	Counter-jet	Vachon et al. (2002)
Pseudomonas					
fluorescens AFT 36	Bovine milk	6-log	$T_{in} = 45$; $p = 150$–250; $T_p = 67$–83	Axial-flow through orifice valve	Hayes et al. (2005)
fluorescens	PBS buffer (pH 7)	6-log	$T_{in} = 25$; $p = 300$; $T_p = 42$	Counter-jet	Wuytack et al. (2002)
Putida 754	Skim milk	3.1-log (lysozyme added) 4.6-log (lysozyme added)	$p = 130$ MPa	Counter-jet	Vannini et al. (2004)

Pseudomonads	Milk	5-log	$p = 200$ MPa; $T_p = 55$	Axial-flow through orifice valve	Smiddy et al. (2007)
Yersinia enterocolitica					
Not reported	PBS buffer (pH 7)	3-log	$T_{in} = 25$; $p = 300$	Counter-jet	Wuytack et al. (2002)
Not reported	PBS buffer (pH 7)	3-log	$p = 130$ MPa	Radial diffuser	Lanciotti et al. (1994)
Not reported	PBS buffer (pH 7)	6-log	$T_{in} = 50$; $p = 250$	Counter-jet	Diels et al. (2003)
Yeast and molds					
Yarrowia lipolitica Y10	PBS buffer (pH 7)	6-log	$p = 130$	Radial diffuser	Lanciotti et al. (1994)
Penicillium ssp	PBS buffer (pH 7)	4-log (after 5 passes)	$p = 200$	Counter-jet	Vachon et al. (2002)
Miscellaneous microorganisms and viruses					
Alicyclobacillus acidoterrestris DSMZ 2498	Malt extract broth	5-log	$p = 170$; $T_p = <55$	Radial diffuser	Bevilacqua et al. (2007)
Entorococcus faecalis	PBS buffer (pH 7)	3-log	$T_{in} = 25$; $p = 250$; $T_p = 42$	Counter-jet	Wuytack et al. (2002)
Lactobacillus plantarum	PBS buffer (pH 7)	4-log	$T_{in} = 25$; $p = 300$; $Tp = 42$	Counter-jet	Wuytack et al. (2002)
Leuconostoc dextranicum	PBS buffer (pH 7)	6-log	$T_{in} = 25$; $p = 300$; $Tp = 42$	Counter-jet	Wuytack et al. (2002)
Lactococcal bacteriophages c2, sk1 and ul36	Milk	3.5-log (after 5 passes)	$T_{in} = 25$; $p = 200$	Counter-jet	Moroni et al. (2002)
Spores - Bacillus subtilis					
PS832	PBS buffer (pH 7)	5-log	$T_{in} = 80$; $p = 350$; $T_p = 144$	Axial-flow through orifice valve	Georget et al. (2014)
A2	Skim milk	3.1-log 4.6-log (lysozyme added)	$p = 130$ MPa	Counter-jet	Vannini et al. (2004)
CECT 4002	Milk	5-log	$T_{in} = 85$; $p = 300$; $T_p = 140$; FR = 8	Axial-flow through orifice valve	Amador Espejo et al. (2014)
Geobacillus stearothermophilus					
ATCC7953	PBS buffer (pH 7)	2-log	$T_{in} = 80$; $p = 350$; $T_p = 144$	Axial-flow through orifice valve	Georget et al. (2014)
CECT 47	Milk	5-log	$T_{in} = 85$; $p = 300$; $T_p = 140$; FR = 8	Axial-flow through orifice valve	Amador Espejo et al. (2014)
Bacillus amyloliquefaciens					
FAD82	Milk PBS buffer (pH 7)	3-log	$T_{in} = 80$; $p = 350$; $T_p = 150$	Axial-flow through orifice valve	Dong et al. (2015)
Bacillus cereus					
Not reported	Soymilk	2.5-log	$T_{in} = 80$; $p = 300$; $T_p = 144$	Axial-flow through orifice valve	Poliseli-Scopel et al. (2014)
CECT5144	Milk	6-log	$T_{in} = 85$; $p = 300$; $T_p = 140$; FR = 8	Axial-flow through orifice valve	Amador Espejo et al. (2014)
***Bacillus* spores**					
B. lincheniformis DSMZ 13	Milk	6-log	$T_{in} = 85$; $p = 300$; $T_p = 140$; FR = 8	Axial-flow through orifice valve	Amador Espejo et al. (2014)
B. sporothermodurans CECT5144	Milk	6-log	$T_{in} = 85$; $p = 300$; $T_p = 140$; FR = 8	Axial-flow through orifice valve	Amador Espejo et al. (2014)
B. coagulans DSMZ2356	Milk	6-log	$T_{in} = 85$; $p = 300$; $T_p = 140$; FR = 8	Axial-flow through orifice valve	Amador Espejo et al. (2014)

Tin – inlet temperature (°C); *p* – homogenization pressure (MPa); *Tp* – product temperature (°C); FR – flow rate L h^{-1}.

during HPH inactivation of *E. coli* K-12. These authors experimentally determined thermal death time at the temperature achieved during HPH, D_{60}, and they assumed a residence time of 20 s. Likewise, Kumar et al. (2009) adopted the same approach in order to separate the thermal contribution during HPH inactivation of *E. coli* K-12. Taylor et al. (2007) and Kumar et al. (2009) concluded that thermal contributions were predominant at homogenization pressures >250 MPa. However, such interpretation must be treated cautiously because the temperature achieved during HPH is due to dissipation of energy of a compressed fluid, which results in large velocity gradients, shear, and other mechanical effects that most likely will have a significant effect on the inactivation. Such interpretations also do not consider the importance of HPH valve geometry on temperature rise. Pathanibul et al. (2009) claimed to separate the effects of shear from the thermal effects by removing the generated heat immediately after homogenization. These authors calculated the equivalent thermal death induced by shear for the inactivation of *E. coli* K-12 and *L. innocua* (ATCC 51742). Strictly speaking, the mechanical effects (shear, velocity gradients, cavitation, and turbulence) cannot be separated from the thermal effects because the increase in temperature after homogenization occurs instantaneously within the fluid due to the dissipation of kinetic energy from a continuous source of energy (pressure).

3.15.8.1.4 Pressure

In general, the microbial inactivation increases with increase in the homogenization pressure. Donsì et al. (2009) pointed out that the inactivation level of *E. coli* and *S. cerevisiae* linearly increased with the homogenization pressure, following a first-order model. These authors used an inlet temperature of 2 °C to minimize thermal effects. Donsì et al. (2009) expressed the inactivation of *E. coli*, *S. cerevisiae*, and *L. delbrueckii* as decimal reduction pressure (D_p), i.e. pressure needed for 1-log reduction. It should be highlighted that the use of D_p relies on linear behavior (first-order with respect to pressure), which is only valid for certain pressure levels and temperatures <50 °C. In addition, current literature on HPH microbial inactivation has not considered the residence time due to equipment limitations. Without the ability to assess different times (after pressure discharge through stage 1 HPH valve), it is not possible to determine the order of the inactivation, which is a fundamental flaw of such an approach. Diels, Wuytack, and Michiels (2003) used quadratic models as a function of inlet temperature and homogenization pressure to predict the inactivation of *S. aureus* and *Y. enterocolitica*. Regardless of the inlet temperature, the inactivation of both microorganisms increased with the homogenization pressure. It is worth to note that the empirical models developed by Diels et al. (2003) do not account for the increase in temperature due to the dissipation of kinetic energy. Sharabi, Okun, and Shpigelman (2018) used ultra-high-pressure homogenization (40–250 MPa and $T_{in} = 25$ °C) in raw milk samples. The authors found the milk samples treated at 200 MPa for 5 cycles reduces ~2.5 log units compared to milk samples treated at 40 MPa for 1 cycle. They also observed that the total bacterial count decreased with increasing pressure and number of cycles at 200 MPa.

3.15.8.1.5 Flow Rate

The product flow rate during HPH treatment governs the extent of pressure generated during treatment, residence time, as well as product temperature after discharge. Most of the studies on microbial inactivation have been performed with lab-scale units operating at low flow rates (<10 L h^{-1}). Donsì et al. (2009) compared a lab-scale (0.7 L h^{-1}) homogenizer (axial-flow through orifice valve) and a pilot-scale homogenizer (120 L h^{-1}) relative to their efficacy in reducing *E. coli* in water. Remarkably, there was no significant difference in the inactivation level between the two units. Based on this observation, Donsì et al. (2009) suggested that those phenomena related to gap opening (shear and elongation) are not among the main contributors to microbial inactivation. It is worth mentioning that despite the differences in the operating flow rate, the homogenization valves in both units are the same and therefore the pressure-volume relationship is the same. Consequently, there is no reason to ignore shear and elongation as the inactivation mechanism.

3.15.8.2 Effects on Enzymes

Pressure can change the structure of enzymes to provide an increase in the number of hydrophobic sites, reveal amino acid and sulfhydryl groups, and induce modifications in enzyme functionality (dos Santos Aguilar et al., 2018). **Table 9** summarizes studies on the HPH effect on different enzymes. In general, HPH may result in activation, inactivation, or no changes in enzyme activity, stability, and functionality.

3.15.8.2.1 Inactivation of Enzymes

Product temperature history has been reported to play a major role during enzymes inactivation in HPH treated beverages. Denaturation of enzymes results in the unfolding of structures with subsequent aggregation due to exposure of the internal groups (Lee et al., 1992). This phenomenon has been demonstrated by Lacroix et al. (2005), who evaluated the effect of a pre-heating step (50 °C/10 min) and multi-pass treatment on pectin methyl esterase (PME) activity in orange juice after HPH treatment (170 MPa) using a counter-jet microchannel valve. A 20% reduction of PME activity after 5 passes was reported at 4 °C initial temperature. Increasing initial temperature to 50 °C resulted in 80% of reduction in the activity of PME enzyme regardless of passes. Similarly, Welti-Chanes et al. (2009) used an HPH (7 L h^{-1}) to inactivate 10%, 50% and 62% of the activity of PME in orange juice after a single pass at 50 MPa/22 °C (inlet temperature), 250 MPa/22 °C, and 250 MPa/45 °C, respectively. Also, these authors reported an enhancement in the inactivation of PME (up to 80%) after 5 passes at 250 MPa. Liu et al. (2010) showed that HPH process decreased gradually the activity of papain. Pressure process between 120 and 180 MPa changed the molecular conformation of the papain amino acids, which decreased the stability of the enzyme (Liu et al., 2010). Carreño et al. (2011) reported 26%

Table 9 Summary of studies on the effect of high-pressure homogenization on different enzymes

Enzyme	*Food matrix*	*Type of valve*	*Conditions*	*Reduction*	*References*
Enzyme inactivation studies					
Pectin methyl esterase (PME)	Orange juice	Counter-jet microchannel	- $T_{in} = 10$ and 50 °C - $P = 170$ MPa - Passes = 1–5	- PME activity of 20% was obtained at $T_{in} = 50$ °C, 170 MPa and 5 passes	Lacroix et al. (2005)
Pectin methyl esterase (PME)	Orange juice	Axial-flow through orifice valve	- $T_{in} = 22$, 35, and 45 °C - $P = 50$, 100, 150, and 250 MPa - Passes = 1–5 - Flow rate = 7 L h^{-1}	- 50% of inactivation after single pass at 250 MPa - 80% of reduction after 5 passes at 250 MPa	Welti-Chanes et al. (2009)
Pectin methyl esterase (PME)	Mandarin juice	Radial-diffuser annular valve	- $T_{in} = 15$ and 30 °C - $P = 30$–120 MPa - Flow rate = 7 L h^{-1}	- 28% of PME activity was reduced at 120 MPa, $T_{in} = 30$ °C and $T_p = 46$ °C	Carreño et al. (2011)
Pectin methyl esterase (PME)	Orange and clementine juice	Radial-diffuser annular valve	- $T_{in} = 21$, 26 and 31 °C - $P = 150$ MPa - $T_p = 58$, 63, and 68 °C - pH = 3.1, 3.5, and 3.9	- PME activity was reduced by 90% at 68 °C and 150 MPa for samples with pH < 3.5	Navarro et al. (2014)
Pectin methyl esterase (PME)	Orange juice	Axial-flow through orifice valve	- $T_{in} = 10$ and 20 °C - $P = 100$, 200, and 300 MPa - Flow rate = 120 L h^{-1}	- 300 MPa (Tp 95 °C) yielded the same inactivation (96%) than 90 °C for 1 min	Velázquez-Estrada et al. (2012)
Pectate lyase (PEL)	Mixture banana puree and water	Radial-diffuser annular valve	- $T_p = 13$, 46, 56, 78 and 100 °C - $P = 150$, 200, 300 and 400 MPa - Flow rate = 200 L h^{-1}	- PEL activity was not detected at pressure levels higher than 150 MPa	Calligaris et al. (2012)
Enzyme	Food matrix	Type of valve	Conditions	Activation/stability	References
Activation and stability of enzymes					
Polyphenol oxidase (PPO)	Chinese pear juice	Counter-jet microchannel	- $P = 80$–180 MPa - Passes = 1–3	- PPO activity increased up to 182% at 180 MPa and 3 passes	Liu et al. (2009b)
Polyphenol oxidase (PPO)	Mushroom PPO solution	Counter-jet microchannel	- $P = 90$–150 MPa - Passes = 1–3	- PPO activity increased up to 110% at 110 MPa and single pass	Liu et al. (2009a)

(Continued)

Table 9 Summary of studies on the effect of high-pressure homogenization on different enzymes—cont'd

Enzyme	*Food matrix*	*Type of valve*	*Conditions*	*Reduction*	*References*
Glucose oxidase (GO)	GO solution (0.05 g L^{-1})	Radial-diffuser annular valve	- $T_{in} = 26$ °C - $P = 0.1$, 75 and 150 MPa - Flow rate = 9 L h^{-1}	- HPH enhanced thermal stability of GO	Tribst et al. (2014)
Trypsin (TR)	Trypsin solution (1 mg mL^{-1})	Counter-jet microchannel	- $P = 40$, 80, 100, 120, 140, and 160 MPa	- TR activity was not affected by homogenization pressure - HPH enhanced thermal stability of TR	Liu et al. (2010)
Glucose oxidase (GO)	GO solution (0.3 g kg^{-1})	Radial-diffuser annular valve	- $T_{in} = 23$ °C - $P = 50$, 100 and 150 MPa - pH = 5.0, 5.7, and 6.5 - Flow rate = 9 L h^{-1}	- HPH enhanced GO stability up to 400% when compared to the native enzyme	Tribst and Cristianini (2012a)
- Amyloglucosidase (AMG) - Glucose oxidase (GO) - Neutral protease (NP)	- AMG: Acetate buffer (pH 5.0) - GO: Phosphate buffer (7.5) - NP: Acetate buffer (pH 4.3)	Radial-diffuser annular valve	- Tin = 23 °C - $P = 150$ and 200 MPa - Flow rate = 9 L h^{-1} - Passes = 1–3	- HPH improved enzyme activity at non-optimum temperature - Multiple passes did not improve enzymes activity	Tribst and Cristianini (2012b)
Calf rennet (CR)	CR solution (1.5%) buffer solution (pH 5.1)	Radial-diffuser annular valve	- $T_{in} = 23$ °C - $P = 50$, 100, 150 and 190 MPa - Flow rate = 9 L h^{-1}	- HPH decreased proteolytic activity - HPH did not affect milk-clotting activity	Leite Júnior et al. (2014)
No effect on enzyme					
Amyloglucosidase (AMG)	AMG solution	Radial-diffuser annular valve	- $T_{in} = 26$ °C - $P = 50$, 100, 150 and 200 MPa - pH = 2.9, 4.3, and 6.5	- HPH slightly increased the activity (5%–8%) of AMG	Tribst and Cristianini (2012c)
β-galactosidase (β-Gal)	β-Gal solution (0.1%)	Radial-diffuser annular valve	- $T_{in} = 8.5$ °C - $P = 50$, 100, and 150 MPa - pH = 6.4; 7.0, and 8.0	- HPH neither affect the activity nor the stability of β-Gal	Tribst et al. (2012)

reduction PME activity in mandarin juice (120 MPa, $T_{in} = 30\ ^{\circ}C$, and $T_p = 45\ ^{\circ}C$) using an HPH with a radial-diffuser annular valve. Navarro et al. (2014) enhanced the inactivation of PME in orange and clementine juice by lowering the pH below 3.5. These authors used an HPH with a radial-diffuser annular valve to inactivate more than 90% of PME activity at 150 MPa and a T_p of 68 °C. Velázquez-Estrada et al. (2012) compared the inactivation of PME in orange juice between a pilot-scale HPH (120 L h^{-1}) and heat pasteurization (90 °C for 1 min). It was found that 300 MPa ($T_{in} = 20\ ^{\circ}C$ and $T_p = 95\ ^{\circ}C$) yielded the same PME inactivation level (96%) as that obtained in thermal pasteurization (90 °C for 1 min). Pectate lyase (PEL) activity is often considered as an indicator of biochemical degradation in some tropical fruits. Calligaris et al. (2012) used a pilot-scale HPH with a radial-diffuser annular valve to inactivate PEL below its detection level in banana juice at pressure levels higher than 150 MPa. Bot et al., 2018 applied HPH process (50–150 MPa and 1–10 passes) for inactivation of polyphenol oxidase (PPO) in apple juice. The authors found 50% reduction in residual PPO activity after 10 passes of 150 MPa.

3.15.8.2.2 Activation of Enzymes

HPH also induces conformational changes of enzymes that may expose active sites, increasing their activity. This has been exemplified by Vannini et al. (2004), who found that the lactoperoxidase enzyme increased its antimicrobial activity against some bacteria inoculated in skim milk, due to changes in the folding and stability during the HPH treatment (75, 100 and 130 MPa and at 37 °C). Liu et al. (2009a,b) subjected pear juice to HPH treatment using a unit with a counter-jet microchannel valve. The activity of polyphenol oxidase (PPO) gradually increased with the homogenization pressure, reaching a maximum activity of 182% at 180 MPa and 3 passes. Similarly, Liu et al. (2009a,b) increased PPO activity up to 110% after single pass at 110 MPa using a counter-jet microchannel valve. These authors evaluated structural changes in PPO through circular dichroism. Significant changes were observed in the PPO spectra, indicating a gradual loss of the secondary structure including α-helix, β-sheet and β-turn. Fluorescence emission spectra showed that tertiary and quaternary structures were partially unfolded, exposing its hydrophilic groups. Similarly, Tribst et al. (2014) found that HPH enhanced the activity of glucose oxidase (GO), an enzyme that catalyzes the oxidation of glucose. These authors observed conformational changes in the molecular structure of GO through fluorescence and circular dichroism, which might be associated with the enhanced activity of GO. It is not clear how the degree of such structural modifications affects the activity or stability of enzymes. An investigation on the effect of HPH on structural conformation of trypsin (TR) revealed the protein unfolding and the formation of disulphide bonds, depending on the homogenization pressure (Liu et al., 2010). Interestingly enough, such structural changes did not significantly influence TR activity but rather enhanced its thermal stability. Similarly, Tribst and Cristianini (2012a) enhanced the stability of GO up to 400% at 150 MPa and T_p of 48 °C in an HPH with radial diffuser annular valve. Tribst et al. (2013) evaluated the effect of HPH on enzyme activity of amyloglucosidase (AMG), glucose oxidase (GO), and neutral protease (NP). These authors found that HPH improved enzyme activity at non-optimum temperature and multiple passes did not further improve enzyme activity. Another study showed that calf rennet treated with HPH reduced its proteolytic activity without altering milk clotting activity (Leite Júnior et al., 2014). More importantly, milk coagulated with enzyme treated with HPH (190 MPa) showed a faster coagulation and higher gel consistence compared to commercial enzymes. Similarly, the activity of amyloglucosidase (AMG) slightly increased with HPH (Tribst and Cristianini, 2012c).

Tribst and Cristianini (2012b) found that neither the activity nor the stability of α-amylase was influenced by HPH (up to 150 MPa) treatment using a radial diffuser annular valve. Similarly, another investigation showed that HPH neither affect the activity nor the stability of β-galactosidase (β-Gal) (Tribst et al., 2012). In general, the HPH treated enzymes have shown important changes upon storage, showing both recovery and decrease of activity. HPH may partially induce unfolding and conformational changes in secondary, tertiary, and quaternary structures, exposing or hindering active sites and thereby increasing or decreasing its activity. A theory that satisfactorily describes the effects of HPH on enzymes has not yet been developed. The effect of HPH on enzyme activity should be evaluated for individual enzymes. Food matrix, homogenization pressure, inlet temperature, product temperature, number of cycles and valve design should be investigated. Many enzyme studies have been conducted with laboratory scale equipment and use multi-pass (recirculation of processed product) as a variable to increase treatment efficacy on enzyme. However, such approach may not be realistic in industrial food manufacturing environment. Research is needed to understand the impact of industrially relevant HPH process conditions on various food formulations containing enzymes.

3.15.9 Stability of Bioactive Compounds

The application of dynamic pressure during HPH may increase the compound's extractability. For that reason, some authors have used HPH as a novel method to obtain, retain, and conserve high value compounds such as polyphenols, flavonoids, anthocyanin, lycopene, so on. Nevertheless, increasing extractability should not be considered as improved nutritional quality. **Table 10** summarizes the effects of homogenization pressure, product temperature, and a number of passes on the concentration and bioaccessibility of selected bioactive compounds.

Colle et al. (2010) studied the combined effects of thermal treatment and HPH on lycopene content and their *in vitro* tomato pulp bioaccessibility. Microscopic images showed that increasing the homogenization pressure strengthened the fiber network, and negatively affected the lycopene bioaccessibility. Svelander et al. (2011) evaluated the *in vitro* carotene bioaccessibility in HPH treated tomato and carrot emulsions. Food matrix and type of carotene influenced the efficacy of HPH for enhancing *in vitro* bioaccessibility. Moelants et al. (2012) correlated the average particle size with carotenoid bioaccessibility. Authors postulated that

Table 10 Effect of high-pressure homogenization on the concentration of bioactive compounds

Compound	*Food matrix*	*Type of valve*	*Conditions*	*Effect*	*References*
Vitamin C	Apple juice	Axial-flow through orifice valve	- $P = 150$ MPa - Flow rate $= 0.7$ L h^{-1} - Passes $= 3$	- HPH did not cause additional losses of vitamin C during storage	Maresca et al. (2011)
Vitamin C	Orange juice	Axial-flow through orifice valve	- $T_{in} = 22$ °C - $P = 50$–250 MPa - Passes $= 1$–5 - Flow rate $= 7$ L h^{-1}	- Vitamin C was not affected by HPH and number passes - Vitamin C remained stable during storage	Welti-Chanes et al. (2009)
Vitamin C	Mango puree	Axial-flow through orifice valve	- $P = 200$ and 300 MPa - Flow rate $= 0.27$ L min-1	- HPH significantly reduced vitamin C	Tribst et al. (2011)
- Vitamin C - Carotenoids - Vitamin A - Flavonoids	Orange juice	Axial-flow through orifice valve	- $T_{in} = 10$ and 20 °C - $P = 100$, 200 and 300 MPa - $T_p = 95$ °C (max) - Flow rate $= 120$ L h^{-1}	- Pressure and product temperature significantly affected the retention of bioactive compounds	Velázquez-Estrada et al. (2013)
- Vitamin C - β-carotene - Retinol equivalent	Apple juice	Axial-flow through orifice valve	- $T_{in} = 4$ and 20 °C - $P = 100$, 200 and 300 MPa - Flow rate $= 100$ L h^{-1}	- HPH did not reduce the content of vitamin C - HPH induced significant losses of β-carotene	Suárez-Jacobo et al. (2011)
Carotenoids (total)	Mandarin juice	Radial-diffuser annular valve	- $T_{in} = 15$ and 30 °C - $P = 30$–120 MPa - Flow rate $= 7$ L h^{-1}	- HPH did not affect the total carotenoid content	Carreño et al. (2011)
Lycopene	Tomato pulp	Radial-diffuser annular valve	- $P = 8$–132 MPa - $T_p = 14$–34 °C	- Residual lycopene after HPH ranges from 87%–102% - No isomerization of lycopene was observed after HPH	Colle et al. (2010)
- Isoflavone - Lysine - Protein digestibility	Soymilk	Axial-flow through orifice valve	- $T_{in} = 55$ and 75 °C - $P = 200$ MPa - $T_p = 105$ and 117 °C - Flow rate $= 100$ L h^{-1}	- HPH did not affect isoflavone profile	Toro-Funes et al. (2014a)
- Phytosterol - Tocopherol - Isoflavone	Soymilk	Axial-flow through orifice valve	- $T_{in} = 55$, 65 and 75 °C - $P = 200$ and 300 MPa - $T_p = 105$–135 °C - Flow rate $= 120$ L h^{-1}	- HPH increased the total phytosterol and isoflavone extractability - HPH decreased the total tocopherol content	Toro-Funes et al. (2014b)
Isoflavone	Soymilk	Axial-flow through orifice valve	- $T_{in} = 75$ °C - $P = 300$ MPa - $T_p = 42$ °C - Flow rate $= 120$ L h^{-1}	- HPH did not affected the total isoflavone content - HPH induced interconversion of isoflavones into β-glucosides	Toro-Funes et al. (2015)
- Lycopene - Lutein - ζ-carotene	Tomato pulp	Radial-diffuser annular valve	- $T_{in} = 4$ °C - $P = 20$, 50, and 100	- HPH decreased bioaccessibility of lycopene, lutein and ζ-carotene	Panozzo et al. (2013)
- α-carotene - β-carotene - lycopene	Emulsion of tomato and carrot	Radial-diffuser annular valve	- $P = 100$ MPa - Passes $= 1$ to 10 (10 M Pa) - Flow rate $= 10$ L h^{-1}	- HPH increased the bioaccessibility by disrupting the cell wall	Svelander et al. (2011)
- β-carotene - lycopene	Emulsion of tomato and carrot	Radial-diffuser annular valve	- $P = 200$ MPa	- Carotenoid bioaccessibility decreased with average particle size	Moelants et al. (2012)

HPH induced destruction of cell walls which in turn releases carotenoids into the micellar phase enhancing its bioaccessibility. Similarly, Panozzo et al. (2013) evaluated the structure of different tomato pulps after HPH and found that pressure yielded a fine fiber network capable of mechanically trapping bioactive compounds. These authors also found that *in vitro* bioaccessibility of lycopene, ζ-carotene and luterin decrease with the homogenization pressure. Tribst et al. (2011) found losses of vitamin C of ∼50% for mango nectar treated at different conditions (100–300 MPa and 73–100 °C). Welti-Chanes et al. (2009) reported that HPH (50–250 MPa and 1–3 passes) did not affect the concentration of vitamin C after processing. Velázquez-Estrada et al. (2013) evaluated the impact of HPH on the concentration of vitamin C, polyphenols, carotenoids and flavonoids in orange juice. The concentration of vitamin C and polyphenols decreased with homogenization pressure and increase in product temperature due to homogenization (∼19 °C/100 MPa). Nevertheless, the concentration of vitamin C and polyphenols obtained after HPH was higher than that obtained in thermal pasteurization (90 °C for 1 min). On the other hand, HPH did not significantly change the total content of carotenoids. Interestingly, individual changes (α-carotene, β-carotene and β-cryptoxanthin) suggest that HPH may favor geometric isomerization. Suárez-Jacobo et al. (2011) compared the impact of HPH (100–300 MPa) and thermal treatment (90 °C for 4 min) on vitamin C, β-carotene and retinol equivalent. While the concentration of vitamin C did not change after HPH, 90% of the vitamin C concentration was lost after thermal treatment. β-carotene and retinol equivalent after HPH were retained 85% and 67%, respectively, while thermal processing retained ∼60% for both compounds. A comparison made on the basis of equivalent lethality (6-log) of *Lactobacillus plantarum* showed that HPH (120 MPa, T_{in} 30 °C) yielded comparable retention of total carotenoids when compared with thermal treatment (77 °C for 10 s) (Carreño et al., 2011).

Toro-Funes et al. (2014b) studied the effects of HPH (200–300 MPa and T_{in} 55–75 °C) on the concentration of total phytosterols, tocopherols and isoflavones in soymilk. It was found that HPH increased the total phytosterol and isoflavone extractability while a significant decrease was observed in the total tocopherol content. Toro-Toro-Funes et al. (2014a) compared the isoflavone profile obtained from HPH (200 MPa, T_{in} 55 and 75 °C, T_p 105 and 107 °C) treated soymilk with the profile from thermally treated (95 °C for 30 s) soymilk. The authors found that the isoflavone profile did not change with HPH treatment. During storage at 4 °C for 21d, an inter-conversion of isoflavone forms, being more pronounced in thermally treated samples. Toro-Funes et al. (2015) evaluated the isoflavone profile of sterilized soymilk during 4 months of storage at 20 °C. It was found that isoflavone converted into β-glucosides faster in UHT treated than HPH treated soymilk.

Zhu et al. (2016) found that the cellular structure of potato peels was altered by HPH (158.58 MPa and 2 passes) and a large number of bioactive components were released. All treatments increased the yields of some phenolic compounds such as ferulic acid, *p*-coumaric, and syringic acid. Li et al. (2017) recovered fucoidan (sulfated polysaccharides) from Nemacystus decipients algae using HPH process (40–100 MPa and cycle times 1–3). The importance of fucoidan compounds is due to their biological activities, which include anti-angiogenic, anti-tumor, anti-inflammatory, antiviral, anticoagulant, and antioxidant activity. The authors found HPH presented a high fucoidan yield with preserving sulfate content. According to the authors the optimal yield was 16.67 ± 0.36%, obtained from 70 MPa for 2 cycles. Xing et al. (2018) used high pressure homogenization method (20–160 MPa and 1–5 passes) in the extraction of sulforaphane from broccoli seeds. Sulforaphane is an isothiocyanate with antioxidant, anti-inflammatory, and anticarcinogenic properties. The authors found the extraction yield was greatly increased after HPH. Where the highest content (2199 μg/g) of sulforaphane was with 35 MPa and 5 passes process, which was three-fold more than the control. According to the authors, the extraction yield increased when the pressure levels increased; however, the highest pressures (>90 MPa) did not present a significant increase in yield extraction.

Jurić et al. (2019) used high-pressure homogenization (HPH) (1–10 passes at 100 MPa) as a disruption method to recover valuable compounds from tomato peels.

3.15.9.1 Emulsification

The benchmark for many formulated liquid foods is the stability upon processing and storage. Emulsions are formulated in order to incorporate immiscible liquids; drops of a given liquid are finely dispersed into an immiscible continuous phase (Walstra, 1993). Although emulsification is an intermediate stage during the manufacturing of liquid foods, it plays a major role determining not only the stability of the whole system but also the final quality of the product. Extensive literature on the significance of emulsification in liquid foods can be found elsewhere (Lee et al., 2013; Walstra, 1993). The formation of emulsions consists of deformation and break-up of liquid droplets, followed by adsorption of surface-active molecules creating a fine colloidal dispersion. Elongation or deformation of droplets is a requisite for break-up since the average diameter of droplets entering the gap is much larger than the gap itself. The newly created emulsion droplets can collide with one another due to Brownian motions and hydrodynamic interactions, leading to the formation of larger droplets coalescence, which is avoided by the addition of stabilizers.

The majority of the literature regarding the effects of HPH on emulsification has been focused on oil in water emulsions. The literature cited in this section should be considered representative and not comprehensive. Emulsification via HPH is a dynamic process controlled by numerous factors that can be classified into four groups:

1) energy density (E_v), which is a function of homogenization pressure and flow rate;
2) flow conditions, including laminar, transitional and turbulent regimes;
3) valve design and configuration, including type of valve, geometry, second stage and number of passes;
4) properties of emulsifying agents, including type and concentration of emulsifiers and stabilizers, viscosity, density, and interfacial properties.

3.15.9.1.1 Effect of Pressure

Desrumaux and Marcand (2002) evaluated the effect of increasing homogenization pressure on emulsion properties and reported significant modifications in the structure of oil in water emulsion with pressure. Authors found that the mean particle size decreased with pressure in an exponential fashion (from 20 to 100 MPa). Increasing pressures further from 100 to 200 MPa increased the mean particle size. Similarly, the application of 210 to 300 MPa homogenization pressures resulted in coalescence of droplets (Desrumaux and Marcand, 2002). Under these conditions, the conformational changes in the protein structure may result in protein losing its emulsifying properties. Similar observations has been reported by Marco-Molés et al. (2012), who found two distinctive effects of homogenization pressure on the stability of oil in water emulsions. Stable emulsions were obtained within the pressure range of 70 to 150 MPa, while destabilization of the emulsions was observed when increasing the pressure up to 250 MPa. In addition, Marco-Molés et al. (2012) showed protein insolubility in those samples treated at 250 MPa, causing coalescence and subsequent separation. Similarly, Martínez-Monteagudo et al. (2017) studied the emulsion stability of nutritional formulations homogenized with HPH and found the existence of a threshold pressure (100–150 MPa) exhibiting significant correlation with product quality and physical stability. It was found that increasing the homogenizing pressure changed the rheological behavior from a shear thinning to a Newtonian behavior.

During emulsification, adsorption and coalescence are perhaps the most critical steps and both occur within a comparable time scale (Jafari et al., 2008). Numerous authors have developed semi-empirical relations to estimate the mean particle size (d_m) or Sauter mean diameter (d_{32}) as a function of energy density or homogenization pressure (Kelemen et al., 2014; Schultz et al., 2004; Stang et al., 2001; Walstra, 1993). Such equations lay within an exponential curve in the form:

$$d_m = E_v^{-b} \tag{14}$$

where b is a constant that depends on the used emulsifying agents. In HPH, the energy density is proportional to the applied homogenization pressure according to (Finke et al., 2014; Kelemen et al., 2014):

$$p \approx E_v \tag{15}$$

3.15.9.1.2 Effect of Flow Conditions

Although variations of **Eq. (14)** provide fairly good predictions of the mean particle size, important deviations have been reported depending on the flow conditions (Kelemen et al., 2014; Schultz et al., 2004). **Eq. (16–18)** were developed to account for the different flow conditions i.e. laminar shear, turbulent viscous and turbulent inertia, respectively.

$$d_m \propto E_v^{-1} \cdot f\left(\frac{n_d}{n_c}\right) \tag{16}$$

$$d_m \propto E_v^{-0.5} \cdot \frac{\gamma}{n_c^{0.5}} \tag{17}$$

$$d_m \propto E_v^{-0.4} \cdot \frac{\gamma^{0.6}}{\rho^{0.2}} \tag{18}$$

Where n_c and n_d are the dynamic viscosity of the dispersed and continuous phase, respectively. A systematic evaluation on the effect of flow conditions on the mean particle size of oil in water emulsions showed considerable differences in the final droplet size depending on the flow regime (laminar, transitional and turbulence) (Kelemen et al., 2014). In **Eq. (19)**, the flow regimes were characterized by means of discharge coefficient (C_d), a dimensionless number. It is worth that droplet size depends on the flow regime, regardless on the energy density. Emulsions homogenized under a laminar regime yielded bigger droplets compared to those homogenized under a transitional and laminar regime. Consequently, flow condition is a primary factor influencing HPH emulsification.

$$C_d = \frac{\dot{V}}{A_c} \cdot \sqrt{\frac{\rho \cdot \left(1 - \left(d/D\right)\right)^4}{2 \cdot \Delta p}} \tag{19}$$

3.15.9.1.2.1 Valve Geometry

Some authors have been investigating the geometry and configuration of the homogenization valve in order to improve the homogenization valves with smaller gaps. However, these authors acknowledged the presence of cavitation may strongly influence the final droplet size, especially when using small gaps. Schlender et al. (2015a) evaluated cavitation patterns in a cylindrical coaxial valve. They employed high speed imaging and acoustic measurements to detect cavitation patterns (jet cavitation, choked cavitation and hydraulic flip). The onset of each cavitation pattern was primarily depended on the valve geometry. The pressure drop or energy density did not significantly alter the onset of the cavitation patterns. It was found that surfactant concentration and disperse phase content influenced neither the existence nor the patterns of cavitation.

Schlender et al. (2015b) investigated the influence of a second homogenization stage during the emulsification of oil in water emulsions. It was found that the droplets are broken up only on the first stage, while the second stage is responsible for the

cavitation patterns. By applying pressure in the second stage, Schlender et al. (2015b) demonstrated that the second stage enhanced the breakage of droplets that occurred in the first stage. This observation was contrary to other researchers who attributed the second stage as the cause of droplet breakup. A minimum droplet size was found with a T_h number of 0.3. These results suggest that an accurate prediction of droplet size should also include the pressure on the second stage and not only the total energy density supplied in stage one. Finke et al. (2014) evaluated the efficiency of a multi orifices valve. Multiple orifices generate different turbulent mixing zones, shortening the coalescence time and therefore improving the emulsification. A consecutive double orifice valve was found to be remarkably efficient and independent of the formulation. The configuration of the valve consisted of a primary orifice (80 μm) and a larger secondary orifice (120 μm) to suppress cavitation according to the T_h number. It is worth mentioning that Finke's valve has only been evaluated up to 100 MPa and a low flow rate of 1 mL s^{-1}. Engineering concepts for the scale-up of a double orifice valve remain to be developed.

The prediction of the mean particle size as a function of energy density is still a significant challenge because the fluid velocity is dramatically accelerated within milliseconds, which creates velocity gradients of large magnitude shifting the balance of adsorption and coalescence. Depending on the valve geometry and configuration, the rate of coalescence can be more predominant than the rate of adsorption. Thus, quantification of droplet break-up and coalescence would provide a more fundamental approach for predicting the speed at which droplet break-up and coalescence occur. However, methods that can distinguish between break-up and coalescence in HPH are scarce (Håkansson and Hounslow, 2013). Taisne et al. (1996) tracked oils between emulsion droplets having different refractive indexes, and they were able to determine the amount of coalescence. Lobo et al. (2002) developed a method using a hydrophobic fluorescent probe for measuring the amount of coalescence occurring during emulsification of oil in water emulsions. It should be highlighted that both methods were developed for low pressure levels (<20 MPa) and lab scale units. In addition, Håkansson and Hounslow (2013) pointed out that both methods used tracer compounds that are hazardous and expensive, making it unsuitable for investigations at pilot scale. Alternatively, Mohan and Narsimhan (1997) calculated the rate of coalescence from the initial formation evolution of the number of drops in the exit stream of the homogenizer when subjected to a step-down in applied pressure. However, this procedure requires multiple steps and it is rather tedious.

Håkansson et al. (2009) studied break-up, adsorption, and coalescence using a dynamic simulation based on population balance equation. The simulations revealed two zones of energy dissipation: (i) a narrow and very intense zone, where only break-up takes place and (ii) a broad and relatively low intensity zone, where coalescence is the predominant phenomena due to drop-drop interactions. Håkansson et al. (2009) also mapped the two energy zones within the homogenization valve as a function of flow coordinate (distance divided by gap height). The break-up zone was found to be significant in a span of 0 to 15 h, while the coalescence zone was mapped within a span of 20–60 h. Similarly, Becker et al. (2014) modeled the droplet break-up in a conventional homogenizer with a population balance equation coupled with CFD simulation. Becker's simulations showed that energy dissipates at high rates inside the gap walls and the rate of dissipation is rapidly reduced in the remainder of the valve. Valve geometry plays a major role on how the energy is dissipated. Therefore, uniform dissipation of energy should not be expected across different valves. Dubbelboer et al. (2014) simulated (population balance equation coupled with CFD) the dissipation of energy into four compartments. Each compartment has its own residence time (ranging from 2 to 0.2 μs), length scale (from 0.12 to 1.38 μm), maximum droplet size (0.15 to 19 μm), volume (0.089 to 0.063 μL) and average turbulent energy dissipation (2.6×1010 to 6.6×10^5 W kg^{-1}). This is a more generic approach that accounts for variations in valve geometry. Unfortunately, experimental validation of the droplet size in each compartment was not possible. Understanding how the energy is dissipated within the homogenization valve is of great relevance since the rate of coalescence can be minimized by shortening the length of the impact zone by engineering the homogenization valve. Despite the insight obtained from CFD simulations, these approaches are only valid within a narrow range of pressure levels (up to 50 MPa) and relatively low flow rates. According to the literature, it is common practice to use multi passes in order to achieve stable droplet size when pressure > 150 MPa are used. Lee et al. (2013) reviewed the effect of multi-passes on emulsification during HPH. Numerous factors are thought to contribute toward emulsification by HPH. Donsì et al. (2012) compared different homogenization valves in a pressure range of 70–280 MPa. These authors performed a sensitivity analysis to evaluate the effect of fluid dynamics and type and concentration of emulsifying agents on emulsification. These authors correlated *We*, and *Re* numbers obtained from different valves with interfacial properties of the emulsifying agents and found that valve geometry plays the most significant role in minimizing the width of the droplet size distributions. These results suggest that the advantage of HPH may be for droplet stabilization against coalescence after disruption. Although encouraging laboratory results have been reported in the literature, applying HPH for emulsification on a large scale still presents many significant challenges. It is worth to note that different threshold of HPH treatment intensity may be required for emulsification, pasteurization or ensuring commercial sterility of a specific product. More research is needed to develop improved HPH valve geometry that can accommodate these unit operations into single treatment step.

The prediction of mean particle size at pressure levels up to 100 MPa has been fairly well described by a power law equation according to Kolmogorov's theory. At high pressure levels (>100 MPa), velocity gradients of large magnitude and other mechanical effects make it difficult to accurately predict the mean particle size. The distinction between adsorption and coalescence is perhaps the most difficult challenge to address since both processes occurred within microseconds and the predominant effect is still unclear. Nevertheless, mechanical effects upon pressure discharge are put to work for emulsification in such a way that by appropriate choice of temperature, homogenization pressure, and food matrix, it may be possible to regulate fat destabilization and adsorbed protein, creating an emulsion with favorable functional attributes. It is believed that HPH treatment facilitates the interactions among various ingredients, offering opportunities for formulated products with improved sensorial perception of salt, sugar, creaminess and related physical properties. However, systematic studies are necessary to understand the phenomenon.

A clear understanding of the mechanisms underlying the interaction between ingredients is essential for obtaining the intended beneficial effect in the food product.

3.15.10 Future Outlook

Homogenization has long being a standard unit operation, and the application of pressure levels higher than 50 MPa is now an industrial reality. Today, a number of operations can be performed by HPH, including cell disruption, mixing, emulsification, and formulation of deserts. Design and configuration of the homogenization valve offer a great potential for applications in tailoring functionality of food components. However, further research for expanding the applicability of HPH are needed, including investigating the effect of geometry and discharge effects on the stability of different compounds and their rheological behavior. Similarly, the impact of HPH on adsorption and coalescence of emulsified particles requires systematic investigation.

3.15.11 Conclusions

A number of emerging applications have been documented for high-pressure homogenization including enzyme inactivation and reactivation, protein denaturation, micro- and nano-emulsification, encapsulation, and extraction of bioactive compounds. Research conducted demonstrated the pasteurization effect of HPH in juices and beverages. More recently, HPH in combination with heat have yielded commercial sterilization by inactivating bacterial spores. The geometry and configuration of the homogenization valve play a major role on how the mechanical effects disperse the structural elements of a given food. By appropriate selection of temperature, pressure, flow regime, and valve geometry, HPH can be used to accomplish a wide range of unit operations.

Acknowledgments

This work has been made possible through the partial financial support from USDA National Institute for Food and Agriculture (HATCH project SD00H607–16).

References

Amador Espejo, G.G., Hernández-Herrero, M.M., Juan, B., Trujillo, A.J., 2014. Inactivation of Bacillus spores inoculated in milk by ultra high pressure homogenization. Food Microbiol. 44, 204–210.

Balasubramaniam, V.M., Martínez-Monteagudo, S.I., Gupta, R., 2015. Principles and application of high pressure–based technologies in the food industry. Annu. Rev .Food Sci. Technol. 6 (1), 435–462.

Bałdyga, J., Pohorecki, R., 1995. Turbulent micromixing in chemical reactors — a review. Chem. Eng. J. Biochem. Eng. J. 58 (2), 183–195.

Becker, P.J., Puel, F., Dubbelboer, A., Janssen, J., Sheibat-Othman, N., 2014. Coupled population balance–CFD simulation of droplet breakup in a high pressure homogenizer. Comput. Chem. Eng. 68, 140–150.

Bevilacqua, A., Cibelli, F., Corbo, M.R., Sinigaglia, M., 2007. Effects of high-pressure homogenization on the survival of Alicyclobacillus acidoterrestris in a laboratory medium. Lett. Appl. Microbiol. 45 (4), 382–386.

Bot, F., Calligaris, S., Cortella, G., Plazzotta, S., Nocera, F., Anese, M., 2018. Study on high pressure homogenization and high power ultrasound effectiveness in inhibiting polyphenoloxidase activity in apple juice. J. Food Eng. 221, 70–76.

Briñez, W.J., Roig-Sagués, A.X., Herrero, M.M.H., López, B.G., 2006a. Inactivation by ultrahigh-pressure homogenization of *Escherichia coli* strains inoculated into orange juice. J. Food Protect. 69 (5), 984–989.

Briñez, W.J., Roig-Sagués, A.X., Herrero, M.M.H., López, B.G., 2006b. Inactivation of Listeria innocua in milk and orange juice by ultrahigh-pressure homogenization. J. Food Protect. 69 (1), 86–92.

Briñez, W.J., Roig-Sagués, A.X., Herrero, M.M.H., López, B.G., 2007. Inactivation of Staphylococcus spp. strains in whole milk and orange juice using ultra high pressure homogenisation at inlet temperatures of 6 and 20 °C. Food Contr. 18 (10), 1282–1288.

Calligaris, S., Foschia, M., Bartolomeoli, I., Maifreni, M., Manzocco, L., 2012. Study on the applicability of high-pressure homogenization for the production of banana juices. LWT - Food Sci. Technol. 45 (1), 117–121.

Carlton, J.S., 2012. Cavitation. In: Carlton, J.S. (Ed.), Marine Propellers and Propulsion. Butterworth-Heinemann, Oxford.

Carreño, J.M., Gurrea, M.C., Sampedro, F., Carbonell, J.V., 2011. Effect of high hydrostatic pressure and high-pressure homogenisation on Lactobacillus plantarum inactivation kinetics and quality parameters of Mandarin juice. Eur. Food Res. Technol. 232 (2), 265–274.

Casoli, P., Vacca, A., Berta, G.L., 2010. A numerical procedure for predicting the performance of high pressure homogenizing valves. Simulat. Model. Pract. Theor. 18 (2), 125–138.

Chahine, G.L., 1997. Numerical simulation of cavitation dynamics. In: Paper Presented at the Proceedings of the 2nd LAAS Conference on Computer Simulation, Beirut, Lebanon.

Clack, A.V., Rejimbal, T.R., Gomez, C. M., inventor, and The Coca-Cola Company, assingee. 1993. Ultra-High Pressure Homogenization of Pasteruized Juice. US5232726.

Colle, I., Van Buggenhout, S., Van Loey, A., Hendrickx, M., 2010. High pressure homogenization followed by thermal processing of tomato pulp: influence on microstructure and lycopene in vitro bioaccessibility. Food Res. Int. 43 (8), 2193–2200.

Cook, E.J., Lagase, A.P., inventors, and PNC Bank National Associaton, MicroFluidics International Corp, assignee. (1985). Apparatus for Forming Emulsions. US4533254A.

Davies, J.T., 1985. Drop sizes of emulsions related to turbulent energy dissipation rates. Chem. Eng. Sci. 40 (5), 839–842.

Desrumaux, A., Marcand, J., 2002. Formation of sunflower oil emulsions stabilized by whey proteins with high-pressure homogenization (up to 350 MPa): effect of pressure on emulsion characteristics. Int. J. Food Sci. Technol. 37 (3), 263–269.

Diels, A.M.J., Callewaert, L., Wuytack, E.Y., Masschalck, B., Michiels, C.W., 2004. Moderate temperatures affect *Escherichia coli* inactivation by high-pressure homogenization only through fluid viscosity. Biotechnol. Prog. 20 (5), 1512–1517.

Diels, A.M.J., Callewaert, L., Wuytack, E.Y., Masschalck, B., Michiels, C.W., 2005a. Inactivation of *Escherichia coli* by high-pressure homogenisation is influenced by fluid viscosity but not by water activity and product composition. Int. J. Food Microbiol. 101 (3), 281–291.
Diels, A.M.J., De Taeye, J., Michiels, C.W., 2005b. Sensitisation of *Escherichia coli* to antibacterial peptides and enzymes by high-pressure homogenisation. Int. J. Food Microbiol. 105 (2), 165–175.
Diels, A.M.J., Wuytack, E.Y., Michiels, C.W., 2003. Modelling inactivation of *Staphylococcus aureus* and Yersinia enterocolitica by high-pressure homogenisation at different temperatures. Int. J. Food Microbiol. 87 (1), 55–62.
Doan, F.J., 1938. Soft curd milk: a critical review of the literature. J. Dairy Sci. 21 (11), 739–756.
Dong, P., Georget, E., Aganovic, K., Heinz, V., Mathys, A., 2015. Ultra high pressure homogenization (UHPH) inactivation of Bacillus amyloliquefaciens spores in phosphate buffered saline (PBS) and milk. Front. Microbiol. 6 (712).
Donsì, F., Ferrari, G., Lenza, E., Maresca, P., 2009. Main factors regulating microbial inactivation by high-pressure homogenization: operating parameters and scale of operation. Chem. Eng. Sci. 64 (3), 520–532.
Donsì, F., Sessa, M., Ferrari, G., 2012. Effect of emulsifier type and disruption chamber geometry on the fabrication of food nanoemulsions by high pressure homogenization. Ind. Eng. Chem. Res. 51 (22), 7606–7618.
dos Santos Aguilar, J.G., Cristianini, M., Sato, H.H., 2018. Modification of enzymes by use of high-pressure homogenization. Food Res. Int. 109, 120–125.
Dubbelboer, A., Janssen, J., Hoogland, H., Mudaliar, A., Maindarkar, S., Zondervan, E., Meuldijk, J., 2014. Population balances combined with Computational Fluid Dynamics: a modeling approach for dispersive mixing in a high pressure homogenizer. Chem. Eng. Sci. 117, 376–388.
Dzurik, J.W., Hair, E.R., Hardy, M.E., and Purves, R.E., inventors, and Procter and Gamble Co, assignee. (1969). Peanut Butter Containing Homogenized Peanut Paste. US3619207A.
Eggers, R., 2012. Basic engineering aspects. In: Eggers, R. (Ed.), Industrial High Pressure Applications, Processes, Equipment And Safety. Wiley-VCH Verlag GmbH & Co, Weinheim.
Endo, H., 1994. Thermodynamic consideration of the cavitation mechanism in homogeneous liquids. J. Acoust. Soc. Am. 95 (5), 2409–2415.
Ferrari, A., 2017. Fluid dynamics of acoustic and hydrodynamic cavitation in hydraulic power systems. Proc. Math. Phys. Eng. Sci. 473 (2199), 20160345-20160345.
Finke, J.H., Niemann, S., Richter, C., Gothsch, T., Kwade, A., Büttgenbach, S., Müller-Goymann, C.C., 2014. Multiple orifices in customized microsystem high-pressure emulsification: the impact of design and counter pressure on homogenization efficiency. Chem. Eng. J. 248, 107–121.
Fisk, W.W., 1924. The Book of Ice-Cream. The MacMillan Comany.
Floury, J., Bellettre, J., Legrand, J., Desrumaux, A., 2004. Analysis of a new type of high pressure homogeniser. A study of the flow pattern. Chem. Eng. Sci. 59 (4), 843–853.
Gaulin, A., inventor, 1904. System for Intimately Mixing Milk. US756953.
Georget, E., Miller, B., Aganovic, K., Callanan, M., Heinz, V., Mathys, A., 2014. Bacterial spore inactivation by ultra-high pressure homogenization. Innovat. Food Sci. Emerg. Technol. 26, 116–123.
Gogate, P.R., Shirgaonkar, I.Z., Sivakumar, M., Senthilkumar, P., Vichare, N.P., Pandit, A.B., 2001. Cavitation reactors: efficiency assessment using a model reaction. AIChE J. 47 (11), 2526–2538.
Gould, I.A., 1941. Effect of certain factors upon lipolysis in homogenized raw milk and cream. J. Dairy Sci. 24 (9), 779–788.
Grandi, S., and Gandini, M., inventors and Niro-Soavi S.p.A., assignee, 2006. Homogenization valve. US 7,144,149.
Håkansson, A., Fuchs, L., Innings, F., Revstedt, J., Bergenståhl, B., Trägårdh, C., 2010. Visual observations and acoustic measurements of cavitation in an experimental model of a high-pressure homogenizer. J. Food Eng. 100 (3), 504–513.
Håkansson, A., Fuchs, L., Innings, F., Revstedt, J., Trägårdh, C., Bergenståhl, B., 2012. Experimental validation of k–ε RANS-CFD on a high-pressure homogenizer valve. Chem. Eng. Sci. 71, 264–273.
Håkansson, A., Hounslow, M.J., 2013. Simultaneous determination of fragmentation and coalescence rates during pilot-scale high-pressure homogenization. J. Food Eng. 116 (1), 7–13.
Håkansson, A., Trägårdh, C., Bergenståhl, B., 2009. Studying the effects of adsorption, recoalescence and fragmentation in a high pressure homogenizer using a dynamic simulation model. Food Hydrocoll. 23 (4), 1177–1183.
Hayes, M.G., Fox, P.F., Kelly, A.L., 2005. Potential applications of high pressure homogenisation in processing of liquid milk. J. Dairy Res. 72 (1), 25–33.
Hinze, J.O., 1955. Fundamentals of the hydrodynamic mechanism of splitting in dispersion processes. AIChE J. 1 (3), 289–295.
Hunziker, O.F., 1935. Condensed Milk and Milk Powder. La Grange, Illinois.
Innings, F., 2015. High-pressure homogenizer design. In: Rayner, M., Dejmek, P. (Eds.), Engineering Aspects of Food Emulsification and Homogenization, first ed. ed. CRC Press, Boca Raton, pp. 149–167.
Innings, F., Hultman, E., Forsberg, F., Prakash, B., 2011. Understanding and analysis of wear in homogenizers for processing liquid food. Wear 271 (9), 2588–2598.
Innings, F., Trägårdh, C., 2005. Visualization of the drop deformation and break-up process in a high pressure homogenizer. Chem. Eng. Technol. 28 (8), 882–891.
Innings, F., Trägårdh, C., 2007. Analysis of the flow field in a high-pressure homogenizer. Exp. Therm. Fluid Sci. 32 (2), 345–354.
Jafari, S.M., Assadpoor, E., He, Y., Bhandari, B., 2008. Re-coalescence of emulsion droplets during high-energy emulsification. Food Hydrocoll. 22 (7), 1191–1202.
Jurić, S., Ferrari, G., Velikov, K.P., Donsì, F., 2019. High-pressure homogenization treatment to recover bioactive compounds from tomato peels. J. Food Eng. 262, 170–180.
Kawaguchi, T., 1971. Entrance loss for turbulent flow without swirl between parallel ddiscs. Bull. JSME 14 (70), 355–363.
Kelemen, K., Schuch, A.C., Schuchmann, H.P., 2014. Influence of flow conditions in high-pressure orifices on droplet disruption of oil-in-water emulsions. Chem. Eng. Technol. 37 (7), 1227–1234.
Kelly, W.J., Muske, K.R., 2004. Optimal operation of high-pressure homogenization for intracellular product recovery. Bioproc. Biosyst. Eng. 27 (1), 25–37.
Kinney, R.R., Pandolfe, W.D., Ferguson, R.D., inventors and APW Homogenizer Group, a Division of APW North America, Inc., assignee, 1999. Homogenization valve. US005749650A.
Kleinig, A.R., Middelberg, A.P.J., 1997. Numerical and experimental study of a homogenizer impinging jet. AIChE J. 43 (4), 1100–1107.
Kumar, P.S., Pandit, A.B., 1999. Modeling hydrodynamic cavitation. Chem. Eng. Technol. 22 (12), 1017–1027.
Kumar, S., Thippareddi, H., Subbiah, J., Zivanovic, S., Davidson, P.M., Harte, F., 2009. Inactivation of *Escherichia coli* K-12 in apple juice using combination of high-pressure homogenization and chitosan. J. Food Sci. 74 (1), M8–M14.
Lacroix, N., Fliss, I., Makhlouf, J., 2005. Inactivation of pectin methylesterase and stabilization of opalescence in orange juice by dynamic high pressure. Food Res. Int. 38 (5), 569–576.
Lanciotti, R., Sinigaglia, M., Angelini, P., Guerzoni, M.E., 1994. Effects of homogenization pressure on the survival and growth of some food spoilage and pathogenic microorganisms. Lett. Appl. Microbiol. 18 (6), 319–322.
Lee, L.L., Niknafs, N., Hancocks, R.D., Norton, I.T., 2013. Emulsification: mechanistic understanding. Trends Food Sci. Technol. 31 (1), 72–78.
Lee, S.-Y., Morr, C.V., Ha, E.Y.W., 1992. Structural and functional properties of caseinate and whey protein isolate as affected by temperature and pH. J. Food Sci. 57 (5), 1210–1229.
Leite Júnior, B.R.d.C., Tribst, A.A.L., Cristianini, M., 2014. Proteolytic and milk-clotting activities of calf rennet processed by high pressure homogenization and the influence on the rheological behavior of the milk coagulation process. Innovat. Food Sci. Emerg. Technol. 21, 44–49.
Li, G.-Y., Luo, Z.-C., Yuan, F., Yu, X.-b., 2017. Combined process of high-pressure homogenization and hydrothermal extraction for the extraction of fucoidan with good antioxidant properties from Nemacystus decipients. Food Bioprod. Process. 106, 35–42.
Liu, W., Liu, J., Liu, C., Zhong, Y., Liu, W., Wan, J., 2009a. Activation and conformational changes of mushroom polyphenol oxidase by high pressure microfluidization treatment. Innovat. Food Sci. Emerg. Technol. 10 (2), 142–147.

Liu, W., Liu, J., Xie, M., Liu, C., Liu, W., Wan, J., 2009b. Characterization and high-pressure microfluidization-induced activation of polyphenol oxidase from Chinese pear (*Pyrus pyrifolia* nakai). J. Agric. Food Chem. 57 (12), 5376–5380.
Liu, W., Zhong, Y.-J., Liu, C.-M., Xie, M.-Y., Guan, B., Yin, M., Chen, T.-T., 2010. The effect of dynamic high pressure microfluidization on the activity of papain. Chin. J. High Press. Phys. 24 (2), 129–135.
Lobo, L., Svereika, A., Nair, M., 2002. Coalescence during emulsification: 1. Method development. J. Colloid Interface Sci. 253 (2), 409–418.
Loo, C.C., Slatter, W.L., Powell, R.W., 1950. A study of the cavitation effect in the homogenization of dairy Products1, 2. J. Dairy Sci. 33 (10), 692–702.
López-Pedemonte, T., Brinẽz, W.J., Roig-Sagués, A.X., Guamis, B., 2006. Fate of *Staphylococcus aureus* in cheese treated by ultrahigh pressure homogenization and high hydrostatic pressure. J. Dairy Sci. 89 (12), 4536–4544.
Marco-Molés, R., Hernando, I., Llorca, E., Pérez-Munuera, I., 2012. Influence of high pressure homogenization (HPH) on the structural stability of an egg/dairy emulsion. J. Food Eng. 109 (4), 652–658.
Maresca, P., Donsì, F., Ferrari, G., 2011. Application of a multi-pass high-pressure homogenization treatment for the pasteurization of fruit juices. J. Food Eng. 104 (3), 364–372.
Martínez-Monteagudo, S.I., Kamat, S., Patel, N., Konuklar, G., Rangavajla, N., Balasubramaniam, V.M., 2017. Improvements in emulsion stability of dairy beverages treated by high pressure homogenization: a pilot-scale feasibility study. J. Food Eng. 193, 42–52.
Martinez-Monteagudo, S.I., Saldaña, M.D.A., 2014. Chemical reactions in food systems at high hydrostatic pressure. Food Eng. Rev. 6 (4), 105–127.
Martinez-Monteagudo, S.I., Yan, B., Balasubramaniam, V.M., 2017. Engineering process characterization of high-pressure homogenization—from laboratory to industrial scale. Food Eng. Rev. 9 (3), 143–169.
McClatchie, J.M., inventor, The Borden Company, assignee, 1930. Valve for Homogenizing Devices. US1763313.
Michaels, A.S., Hauser, E.A., 1951. Interfacial tension at elevated pressure and temperature. II. Interfacial properties of hydrocarbon–water systems. J. Phys. Chem. 55 (3), 408–421.
Miller, J., Rogowski, M., Kelly, W., 2002. Using a CFD model to understand the fluid dynamics promoting *E. coli* breakage in a high-pressure homogenizer. Biotechnol. Prog. 18 (5), 1060–1067.
Moelants, K.R.N., Lemmens, L., Vandebroeck, M., Van Buggenhout, S., Van Loey, A.M., Hendrickx, M.E., 2012. Relation between particle size and carotenoid bioaccessibility in carrot- and tomato-derived suspensions. J. Agric. Food Chem. 60 (48), 11995–12003.
Mohan, S., Narsimhan, G., 1997. Coalescence of protein-stabilized emulsions in a high-pressure homogenizer. J. Colloid Interface Sci. 192 (1), 1–15.
Mohr, K.H., 1987. High-pressure homogenization. Part I. Liquid-liquid dispersion in turbulence fields of high energy density. J. Food Eng. 6 (3), 177–186.
Moroni, O., Jean, J., Autret, J., Fliss, I.I., 2002. Inactivation of lactococcal bacteriophages in liquid media using dynamic high pressure. Int. Dairy J. 12 (11), 907–913.
Naidu, D.V.P., Rajan, R., Kumar, R., Gandhi, K.S., Arakeri, V.H., Chandrasekaran, S., 1994. Modelling of a batch sonochemical reactor. Chem. Eng. Sci. 49 (6), 877–888.
Nakayama, Y., 1964. Action of the fluid in the air-micrometer : 3rd report, characteristics of double-disc nozzle No.1, in the case of compressibility being ignored. Trans. Jpn Soc. Mechan. Eng. 30 (210), 202–210.
Navarro, J.L., Izquierdo, L., Carbonell, J.V., Sentandreu, E., 2014. Effect of pH, temperature and maturity on pectinmethylesterase inactivation of citrus juices treated by high-pressure homogenization. LWT - Food Sci. Technol. 57 (2), 785–788.
Panagiotou, T., Fisher, R., 2012. Improving product quality with entrapped stable emulsions: from theory to industrial application. Challenges 3 (2), 84–113.
Pandolfe, W.D., 1982. Development of the new Gaulin micro-Gap™ homogenizing valve. J. Dairy Sci. 65 (10), 2035–2044.
Panozzo, A., Lemmens, L., Van Loey, A., Manzocco, L., Nicoli, M.C., Hendrickx, M., 2013. Microstructure and bioaccessibility of different carotenoid species as affected by high pressure homogenisation: a case study on differently coloured tomatoes. Food Chem. 141 (4), 4094–4100.
Patazca, E., Koutchma, T., Balasubramaniam, V.M., 2007. Quasi-adiabatic temperature increase during high pressure processing of selected foods. J. Food Eng. 80 (1), 199–205.
Pathanibul, P., Taylor, T.M., Davidson, P.M., Harte, F., 2009. Inactivation of *Escherichia coli* and Listeria innocua in apple and carrot juices using high pressure homogenization and nisin. Int. J. Food Microbiol. 129 (3), 316–320.
Phipps, L.W., 1975. The fragmentation of oil drops in emulsions by a high-pressure homogenizer. J. Phys. D Appl. Phys. 8 (4), 448–462.
Poliseli-Scopel, F.H., Hernández-Herrero, M., Guamis, B., Ferragut, V., 2014. Sterilization and aseptic packaging of soymilk treated by ultra high pressure homogenization. Innovat. Food Sci. Emerg. Technol. 22, 81–88.
Rosa, R.M.S., 2006. Turbulence theories. In: Françoise, J.P., Naber, G.L., Tsun, T.S. (Eds.), Encyclopedia of Mathematical Physics, first ed. Academic Press, Oxford.
Rovinsky, L.A., 1994. The analysis and calculation of the efficiency of a homogenizing valve. J. Food Eng. 23 (4), 429–448.
Schlender, M., Minke, K., Spiegel, B., Schuchmann, H.P., 2015a. High-pressure double stage homogenization processes: influences of plant setup on oil droplet size. Chem. Eng. Sci. 131, 162–171.
Schlender, M., Spengler, A., Schuchmann, H.P., 2015b. High-pressure emulsion formation in cylindrical coaxial orifices: influence of cavitation induced pattern on oil drop size. Int. J. Multiphas. Flow 74, 84–95.
Schultz, S., Wagner, G., Urban, K., Ulrich, J., 2004. High-pressure homogenization as a process for emulsion formation. Chem. Eng. Technol. 27 (4), 361–368.
Sharabi, S., Okun, Z., Shpigelman, A., 2018. Changes in the shelf life stability of riboflavin, vitamin C and antioxidant properties of milk after (ultra) high pressure homogenization: direct and indirect effects. Innovat. Food Sci. Emerg. Technol. 47, 161–169.
Shirgaonkar, I.Z., Lothe, R.R., Pandit, A.B., 1998. Comments on the mechanism of microbial cell disruption in high-pressure and high-speed devices. Biotechnol. Prog. 14 (4), 657–660.
Smiddy, M.A., Martin, J.-E., Huppertz, T., Kelly, A.L., 2007. Microbial shelf-life of high-pressure-homogenised milk. Int. Dairy J. 17 (1), 29–32.
Stang, M., Schuchmann, H., Schubert, H., 2001. Emulsification in high-pressure homogenizers. Eng. Life Sci. 1 (4), 151–157.
Stevenson, M.J., Chen, X.D., 1997. Visualization of the flow patterns in a high-pressure homogenizing valve using a CFD package. J. Food Eng. 33 (1), 151–165.
Suárez-Jacobo, Á., Rüfer, C.E., Gervilla, R., Guamis, B., Roig-Sagués, A.X., Saldo, J., 2011. Influence of ultra-high pressure homogenisation on antioxidant capacity, polyphenol and vitamin content of clear apple juice. Food Chem. 127 (2), 447–454.
Suslick, K.S., Mdleleni, M.M., Ries, J.T., 1997. Chemistry induced by hydrodynamic cavitation. J. Am. Chem. Soc. 119 (39), 9303–9304.
Svelander, C.A., Lopez-Sanchez, P., Pudney, P.D.A., Schumm, S., Alminger, M.A.G., 2011. High pressure homogenization increases the in vitro bioaccessibility of α- and β-carotene in carrot emulsions but not of lycopene in tomato emulsions. J. Food Sci. 76 (9), H215–H225.
Tahiri, I., Makhlouf, J., Paquin, P., Fliss, I., 2006. Inactivation of food spoilage bacteria and *Escherichia coli* O157:H7 in phosphate buffer and orange juice using dynamic high pressure. Food Res. Int. 39 (1), 98–105.
Taisne, L., Walstra, P., Cabane, B., 1996. Transfer of oil between emulsion droplets. J. Colloid Interface Sci. 184 (2), 378–390.
Taylor, T.M., Roach, A., Black, D.G., Davidson, P.M., Harte, F., 2007. Inactivation of *Escherichia coli* K-12 exposed to pressures in excess of 300 MPa in a high-pressure homogenizer. J. Food Protect. 70 (4), 1007–1010.
Tennekes, H., Lumley, J.L., 1972. *A First Course in Turbulence*: A First Course in Turbulence. The MIT Press, Massachusetts, MA.
Theophilus, D.R., Hansen, H.C., Spencer, M.B., 1934. Influence of homogenization on the curd tension of milk. J. Dairy Sci. 17 (7), 519–524.
Thiebaud, M., Dumay, E., Picart, L., Guiraud, J.P., Cheftel, J.C., 2003. High-pressure homogenisation of raw bovine milk. Effects on fat globule size distribution and microbial inactivation. Int. Dairy J. 13 (6), 427–439.
Toro-Funes, N., Bosch-Fusté, J., Latorre-Moratalla, M.L., Veciana-Nogués, M.T., Vidal-Carou, M.C., 2015. Isoflavone profile and protein quality during storage of sterilised soymilk treated by ultra high pressure homogenisation. Food Chem. 167, 78–83.
Toro-Funes, N., Bosch-Fusté, J., Veciana-Nogués, M.T., Vidal-Carou, M.C., 2014a. Changes of isoflavones and protein quality in soymilk pasteurised by ultra-high-pressure homogenisation throughout storage. Food Chem. 162, 47–53.

Toro-Funes, N., Bosch-Fusté, J., Veciana-Nogués, M.T., Vidal-Carou, M.C., 2014b. Effect of ultra high pressure homogenization treatment on the bioactive compounds of soya milk. Food Chem. 152, 597–602.
Tribst, A.A.L., Augusto, P.E.D., Cristianini, M., 2012. The effect of high pressure homogenization on the activity of a commercial β-galactosidase. J. Ind. Microbiol. Biotechnol. 39 (11), 1587–1596.
Tribst, A.A.L., Augusto, P.E.D., Cristianini, M., 2013. Multi-pass high pressure homogenization of commercial enzymes: effect on the activities of glucose oxidase, neutral protease and amyloglucosidase at different temperatures. Innovat. Food Sci. Emerg. Technol. 18, 83–88.
Tribst, A.A.L., Cota, J., Murakami, M.T., Cristianini, M., 2014. Effects of high pressure homogenization on the activity, stability, kinetics and three-dimensional conformation of a glucose oxidase produced by Aspergillus Niger. PLoS One 9 (7), e103410.
Tribst, A.A.L., Cristianini, M., 2012a. Changes in commercial glucose oxidase activity by high pressure homogenization. Innovat. Food Sci. Emerg. Technol. 16, 355–360.
Tribst, A.A.L., Cristianini, M., 2012b. High pressure homogenization of a fungi α-amylase. Innovat. Food Sci. Emerg. Technol. 13, 107–111.
Tribst, A.A.L., Cristianini, M., 2012c. Increasing fungi amyloglucosidase activity by high pressure homogenization. Innovat. Food Sci. Emerg. Technol. 16, 21–25.
Tribst, A.A.L., Franchi, M.A., de Massaguer, P.R., Cristianini, M., 2011. Quality of mango nectar processed by high-pressure homogenization with optimized heat treatment. J. Food Sci. 76 (2), M106–M110.
Trout, G.M., 1963. Official acceptance of homogenized milk in the United States. J. Dairy Sci. 46 (4), 342–345.
Trout, M.G., 1950. Homogenized Milk. Michigan State College Press, East Lansing.
Vachon, J.F., Kheadr, E.E., Giasson, J., Paquin, P., Fliss, I., 2002. Inactivation of foodborne pathogens in milk using dynamic high pressure. J. Food Protect. 65 (2), 345–352.
van Wijngaarden, L., 2016. Mechanics of collapsing cavitation bubbles. Ultrason. Sonochem. 29, 524–527.
Vannini, L., Lanciotti, R., Baldi, D., Guerzoni, M.E., 2004. Interactions between high pressure homogenization and antimicrobial activity of lysozyme and lactoperoxidase. Int. J. Food Microbiol. 94 (2), 123–135.
Velázquez-Estrada, R.M., Hernández-Herrero, M.M., Guamis-López, B., Roig-Sagués, A.X., 2012. Impact of ultra high pressure homogenization on pectin methylesterase activity and microbial characteristics of orange juice: a comparative study against conventional heat pasteurization. Innovat. Food Sci. Emerg. Technol. 13, 100–106.
Velázquez-Estrada, R.M., Hernández-Herrero, M.M., Rüfer, C.E., Guamis-López, B., Roig-Sagués, A.X., 2013. Influence of ultra high pressure homogenization processing on bioactive compounds and antioxidant activity of orange juice. Innovat. Food Sci. Emerg. Technol. 18, 89–94.
Walstra, P., 1993. Principles of emulsion formation. Chem. Eng. Sci. 48 (2), 333–349.
Welti-Chanes, J., Ochoa-Velasco, C.E., Guerrero-Beltrán, J.Á., 2009. High-pressure homogenization of orange juice to inactivate pectinmethylesterase. Innovat. Food Sci. Emerg. Technol. 10 (4), 457–462.
Wuytack, E.Y., Diels, A.M.J., Michiels, C.W., 2002. Bacterial inactivation by high-pressure homogenisation and high hydrostatic pressure. Int. J. Food Microbiol. 77 (3), 205–212.
Xing, J.-j., Cheng, Y.-l., Chen, P., Shan, L., Ruan, R., Li, D., Wang, L.-j., 2018. Effect of high-pressure homogenization on the extraction of sulforaphane from broccoli (*Brassica oleracea*) seeds. Powder Technol. 358, 103–109.
Zhu, X., Cheng, Y., Chen, P., Peng, P., Liu, S., Li, D., Ruan, R., 2016. Effect of alkaline and high-pressure homogenization on the extraction of phenolic acids from potato peels. Innovat. Food Sci. Emerg. Technol. 37, 91–97.